

Article

# Minute-Cadence Observations of the LAMOST Fields with the TMTS: IV— Catalog of Cataclysmic Variables from the First 3-yr Survey

Qichun Liu <sup>1</sup>, Jie Lin <sup>1,2,3,\*</sup>, Xiaofeng Wang <sup>1,\*</sup>, Zhibin Dai <sup>4,5</sup>, Yongkang Sun <sup>6,7</sup>, Gaobo Xi <sup>1</sup>, Jun Mo <sup>1</sup>, Jialian Liu <sup>1</sup>, Shengyu Yan <sup>1</sup>, Alexei V. Filippenko <sup>8</sup>, Thomas G. Brink <sup>8</sup>, Yi Yang <sup>1,8</sup>, Kishore C. Patra <sup>8</sup>, Yongzhi Cai <sup>4,5,9</sup>, Zhihao Chen <sup>1</sup>, Liyang Chen <sup>1</sup>, Fangzhou Guo <sup>1</sup>, Xiaojun Jiang <sup>7,10,11</sup>, Gaici Li <sup>1</sup>, Wenxiong Li <sup>10</sup>, Weili Lin <sup>12</sup>, Cheng Miao <sup>1</sup>, Xiaoran Ma <sup>1</sup>, Haowei Peng <sup>1</sup>, Qiqi Xia <sup>1</sup>, Danfeng Xiang <sup>1</sup> and Jicheng Zhang <sup>13</sup>

- <sup>1</sup> Physics Department and Tsinghua Center for Astrophysics, Tsinghua University, Beijing 100084, China; lqc22@mails.tsinghua.edu.cn (Q.L.); hgb18@mails.tsinghua.edu.cn (G.X.); moj20@mails.tsinghua.edu.cn (J.M.); liu-jl22@mails.tsinghua.edu.cn (J.L.); yansy19@mails.tsinghua.edu.cn (S.Y.); yi.yang@berkeley.edu (Y.Y.); chenzh18@mails.tsinghua.edu.cn (Z.C.); chenly23@mails.tsinghua.edu.cn (L.C.); gzf20@mails.tsinghua.edu.cn (F.G.); lgc21@mails.tsinghua.edu.cn (G.L.); miaoc19@mails.tsinghua.edu.cn (C.M.); maxr20@mails.tsinghua.edu.cn (X.M.); phw23@mails.tsinghua.edu.cn (H.P.); xiaqiqi@mail.tsinghua.edu.cn (Q.X.); xiangdf@mail.tsinghua.edu.cn (D.X.)
- <sup>2</sup> CAS Key Laboratory for Research in Galaxies and Cosmology, Department of Astronomy, University of Science and Technology of China, Hefei 230026, China
- <sup>3</sup> School of Astronomy and Space Sciences, University of Science and Technology of China, Hefei 230026, China
- <sup>4</sup> Yunnan Observatories, Chinese Academy of Sciences, Kunming 650216, China; zhibin\_dai@ynao.ac.cn (Z.D.); caiyongzhi@ynao.ac.cn (Y.C.)
- <sup>5</sup> Key Laboratory for the Structure and Evolution of Celestial Objects, Chinese Academy of Sciences, Kunming 650216, China
- <sup>6</sup> National Astronomical Observatories, Chinese Academy of Sciences, Beijing 100101, China; sunyk@bao.ac.cn
- <sup>7</sup> School of Astronomy and Space Science, University of Chinese Academy of Sciences, Beijing 100049, China; xjjiang@bao.ac.cn
- <sup>8</sup> Department of Astronomy, University of California, Berkeley, CA 94720-3411, USA; aphilippenko@berkeley.edu (A.V.F.); tgbrink@berkeley.edu (T.G.B.); kcpatra@berkeley.edu (K.C.P.)
- <sup>9</sup> International Centre of Supernovae, Yunnan Key Laboratory, Kunming 650216, China
- <sup>10</sup> CAS Key Laboratory of Optical Astronomy, National Astronomical Observatories, Chinese Academy of Sciences, Beijing 100101, China; li-wx15@tsinghua.org.cn
- <sup>11</sup> Center for Astronomical Mega-Science, Chinese Academy of Sciences, 20A Datun Road, Chaoyang District, Beijing 100101, China
- <sup>12</sup> Department of Astronomy, Xiamen University, Xiamen 361005, China; linwl@xmu.edu.cn
- <sup>13</sup> Department of Astronomy, Beijing Normal University, Beijing 100875, China; jczhang@bnu.edu.cn
- \* Correspondence: linjie2019@ustc.edu.cn (J.L.); wang\_xf@mail.tsinghua.edu.cn (X.W.)

**Abstract:** The Tsinghua University–Ma Huateng Telescopes for Survey (TMTS) started to monitor the LAMOST plates in 2020, leading to the discovery of numerous short-period eclipsing binaries, peculiar pulsators, flare stars, and other variable objects. Here, we present the uninterrupted light curves for a sample of 64 cataclysmic variables (CVs) observed/discovered using the TMTS during its first three-year observations, and we introduce new CVs and new light-variation periods (from known CVs) revealed through the TMTS observations. Thanks to the high-cadence observations of TMTS, diverse light variations, including superhumps, quasi-periodic oscillations, large-amplitude orbital modulations, and rotational modulations, are able to be detected in our CV samples, providing key observational clues for understanding the fast-developing physical processes in various CVs. All of these short-timescale light-curve features help further classify the subtypes of CV systems. We highlight the light-curve features observed in our CV sample and discuss further implications of minute-cadence light curves for CV identifications and classifications. Moreover, we examine the H $\alpha$  emission lines in the spectra from our nonmagnetic CV samples (i.e., dwarf novae and nova-like subclasses) and find that the distribution of H $\alpha$  emission strength shows significant differences between the sources with orbital periods above and below the period gap, which agrees with the trend seen from the SDSS nonmagnetic CV sample.

arXiv:2408.12104v1 [astro-ph.SR] 22 Aug 2024



**Citation:** Liu, Q.; Lin, J.; Wang, X.; Dai, Z.; Sun, Y.; Xi, G.; Mo, J.; Liu, J.; Yan, S.; Filippenko, A.V.; et al. Minute-Cadence Observations of the LAMOST Fields with the TMTS: IV—Catalog of Cataclysmic Variables from the First 3-yr Survey. *Universe* **2024**, *1*, 0. <https://doi.org/>

Academic Editor:

Received: 18 July 2024

Revised: 16 August 2024

Accepted: 20 August 2024

Published:



**Copyright:** © 2024 by the authors. Licensee MDPI, Basel, Switzerland. This article is an open access article distributed under the terms and conditions of the Creative Commons Attribution (CC BY) license (<https://creativecommons.org/licenses/by/4.0/>).

**Keywords:** surveys; cataclysmic variables; evolution; accretion

## 1. Introduction

Cataclysmic variables (CVs) are semidetached binaries consisting of a white dwarf (WD) and a Roche-lobe-overflowing low-mass companion that is usually on or near the late-type main sequence. Observations of CVs provide opportunities to study accretion theories, the physics of compact objects, and the evolution of WD binaries, as some of them may ultimately end as Type Ia supernova explosions [1,2] or form an AM CVn system with mHz gravitational waves (GWs) detected via space-born GW observatories [3–6].

In CV systems, material from the donor star will be accreted onto the WD companion through the inner Lagrangian point  $L_1$  [7] and form a surrounding accretion disc or fall into the magnetic poles of the WD, depending on the strength of the WD's magnetic field. Nonmagnetic CVs have two main subclasses, namely dwarf novae (DNe) and nova-like variables (NLs), which are both disk-dominant systems. The dominant difference between them is that the DN subclass undergoes recurrent outbursts, while the NL subclass does not [8]. In comparison, magnetic CVs can also be divided into two subclasses, intermediate polars (IPs, or DQ Her) with weak magnetic fields and polars (or AM Her/AM) with stronger magnetic fields (e.g., 10–200 MG) [9]. The magnetic fields of IPs are not strong enough to prevent the formation of a disk, while their accretion mode may switch among different states (i.e., high/low state) [10]. Owing to the strong magnetic fields of polars, their accreted material follows the magnetic field lines to reach directly near the WD's magnetic poles and form accretion columns. The collision of subsonic falling flows against the WD photosphere leads to the formation of a shock, and the shock-heated emission contributes significantly to the radiation of polars [11,12].

Superhumps are the periodic light-curve modulations of CVs with a photometric period comparable to their orbital period and an amplitude of about 0.3–0.4 mag [7]. The modulation period is slightly longer than the orbital period in positive superhumps (pSHs), while the modulation period is shorter than the orbital period in negative superhumps (nSHs) [13]. The pSHs were proposed to be induced via tidal instability in the disk [14]. Tidal interaction with the secondary will impose an elliptical deformation to the disc [15] when it expands to the 3:1 resonance region during the outburst. The precession of the eccentric accretion disk results in the light-curve modulations seen in those pSHs. In contrast, the nSHs are believed to be the retrograde precession of a tilted disk [16,17].

A prominent property of the CV population is the 2–3 H orbital period gap [18]. In binary evolution theories, angular-momentum loss (AML) can drive the orbital contraction of CVs. Magnetic braking is the dominant driving mechanism of AML for long-period CVs, leading to a typical mass-transfer rate of  $\dot{M} \approx 10^{-9}–10^{-8} M_{\odot} \text{ yr}^{-1}$  [19], while GW radiation is the dominant AML mechanism for those short-period CVs, and it induces a mass-transfer rate of  $\dot{M} \approx 5 \times 10^{-11} M_{\odot} \text{ yr}^{-1}$  [20].

The spectra of CV systems usually show  $H\alpha$  emission, which is thought to be related to the optically thin outer regions of the disks [21]. High-inclination CV systems even exhibit obvious double-peaked profiles due to Doppler broadening. However, during outburst, DNe tend to show narrow Balmer emission lines with broad absorption wings, which can be explained by a hot, optically thick disk with a relatively cool and optically thin outer region [22]. Sarty and Wu [23] adopted a discriminant function and principal-component analysis to study the ratios of Balmer emission lines, and they found that the discriminant function can separate DNe from other subclasses.

Based on the well-sampled light curves from several telescopes like *Kepler* [24] and the *Transiting Exoplanet Survey Satellite* (*TESS*; Ricker et al. [25]), light variations intrinsic to CVs have been examined [13,26,27], which helps improve our understanding of accretion instability. TMTS can also provide well-sampled light curves for CVs; it is a multitube telescope system consisting of four 40 cm optical telescopes, and it has a field of view

(FoV) of up to about  $18 \text{ deg}^2$  [28]. This facility has discovered/monitored over 1100 short-period variable sources during the first two-year monitoring of the Large Sky Area Multi-Object Fiber Spectroscopic Telescope (LAMOST; Cui et al. [29], Zhao et al. [30]) skyfields, including eclipsing binaries, pulsating stars, cataclysmic variables, and so on [31–36]. This paper aims to release the light curves of CVs and the candidates identified in the first 3 yr, and it presents the analysis of their periodicities, light-curve features, and spectroscopic properties.

## 2. Observations and Data Analysis

### 2.1. TMTS CV Sample

In the first 3 yr survey, TMTS covered a total of  $6977 \text{ deg}^2$  (449 LAMOST/TMTS plates with more than 100 visits), and it produced 19,099,266 uninterrupted light curves with at least 100 valid measurements for about 20 million sources. After cross-matching the CV catalog that contains 5478 CVs and CV candidates from the SIMBAD database [37] and other works in the literature [38–41], we obtained the light curves for a total of 57 CVs and 5 CV candidates. Additionally, this work includes two new CV candidates that were first discovered through TMTS—TMTS J04405040+6820355 and TMTS J06183036+5105550. Among the 64 CV samples, 57 have been included in the International Variable Star Index (VSX) [42], with classifications recorded as 29 DNe, 12 NLs, 11 IPs, and 5 AMs.

Note that most of the samples were uninterruptedly observed within single nights except for five sources that were monitored on two separate nights. The procedures of TMTS photometry and calibration are described by Lin et al. [31]. Uninterrupted light curves of the 64 CVs are shown in Figures A1–A5. These light curves typically span 4–12 h, with a cadence of about 1 min. For those known CVs, we also labeled the IAU-sanctioned names.

Benefiting from our observation strategy, among the 64 samples, spectra of 27 are available from the LAMOST DR7. We obtained spectra of an additional 29 objects with the Xinglong 2.16 m telescope (XLT) and the Lick 3 m Shane telescope (LST). Nevertheless, spectroscopic data are still absent for seven objects of our collected samples. Figure A6 shows the spectra of our 57 CV samples. Here, we give brief introductions to some candidates listed in Table 1. TMTS J03394099+4148057 was identified as an NL candidate [43] with a radial-velocity period of 3.54 h [44]. Our spectrum of this object revealed the presence of prominent H $\alpha$   $\lambda$ 6563 and He I  $\lambda$ 6678 and  $\lambda$ 7065 emission lines. TMTS J09011350+1447046 is a CV candidate that was first discovered by Szkody et al. [45], and its LAMOST spectrum exhibits a broad, moderately strong H $\alpha$  emission [41]. TMTS J07200739+4516113 was initially discovered by Denisenko [46], and it has been suggested to be polar, according to the helium emission features seen in the LAMOST spectra [41] or its large amplitude of light variation [35]. Owing to the lack of detailed analysis and constraints on the accretion structure, we tentatively treat it as a CV candidate in this work.

**Table 1.** Catalog of cataclysmic variables from the TMTS observations.

Name	Start Time (MJD)	$P_{\text{pho}}$ (min)	Amplitude (mag)	Feature	VSX Name	Reference
Dwarf novae						
TMTS J00060995+5558501	59886.42805				FI Cas	1
TMTS J01010887+4323259	59877.42796				IW And	1
TMTS J01043552+4117576	59877.44097	$145.0 \pm 0.3$	0.165	L,R	RX And	1
TMTS J01101317+6004349	59509.46110				HT Cas	1
TMTS J01153217+3737354	59876.43408				FO And	1
TMTS J01275052+3808122	59876.47894				1RXS J0127+38	1
TMTS J02135093+5822527	59596.43877				TZ Per	1
TMTS J02262311+7118314	59210.41097				AM Cas	1

Table 1. Cont.

Name	Start Time (MJD)	$P_{pho}$ (min)	Amplitude (mag)	Feature	VSX Name	Reference
Dwarf novae						
TMTS J02500008+3739219	59194.43101				PY Per	1
TMTS J03124571+3042477	59199.42001				CRTS J0312+30	2
TMTS J03321548+5847219 *	59899.67009				AF Cam	1
-	59207.41269				-	-
TMTS J04023898+4250447 *	59548.42925				V1024 Per	3
-	59548.42836				-	-
TMTS J04083502+5114484	59943.41288	$208.00 \pm 1.45$	1.344	H	FO Per	1
TMTS J04184443+5107313 *	58877.44968				NS Per	1
-	59943.41273	$110.98 \pm 1.33$	0.177	L	-	-
TMTS J04260927+3541442	59554.42448				MASTER OT J0426+35	4
TMTS J04463363+4857559	58852.42751				ASASSN-15rs	5
TMTS J05235177+0100303	59249.43854	$135.83 \pm 3.39$	0.213	L	BI Ori	1
TMTS J05581781+6753456	59598.45463	$46.4 \pm 0.4$	0.300	L	LU Cam	1
TMTS J06132238+4744248	59202.41699				SS Aur	1
TMTS J07485955+3125121	59281.46741	$82.1 \pm 0.8$	0.429	E	SDSS J0748+31	5
TMTS J08442711+1252322 *	59204.65922			E	AC Cnc	1
-	58898.47159			E	-	1
TMTS J08534425+5748402	59216.69161				BZ UMa	1
TMTS J09121621+5053531	59617.68575	$77.9 \pm 0.9$	0.339	L	DI UMa	1
TMTS J10020745+3351005	59941.67607			R	RU LMi	1
TMTS J10043481+6629148	59685.52063	$133.76 \pm 2.06$	0.167	L	LN UMa	1
TMTS J10202651+5304330	59631.73682				KS UMa	1
TMTS J10543054+3006090	59248.54145				SX LMi	1
TMTS J10565691+4941183	59672.48447	$193.12 \pm 1.55$	0.295	L	CY UMa	1
TMTS J12393204+2108063	59676.48460			E	IR Com	1
Intermediate polars						
TMTS J00225764+6141076	59507.45075	$9.372 \pm 0.005$	0.239	R,L	V1033 Cas	1
TMTS J00284893+5917207	59181.43487				V709 Cas	1
TMTS J00551974+4612566 *	59873.51739				V515 And	6
-	59869.43510	$203.1 \pm 0.9$	0.112	L	-	-
TMTS J03311195+4354154	59530.42598				GK Per	1
TMTS J05474838+2835104	59235.42950				FS Aur	1
TMTS J06251631+7334386	59597.42651	$19.785 \pm 0.009$	0.209	R,L	MU Cam	1
TMTS J06274641+0148100	59250.44675			E	V902 Mon	7
TMTS J07511729+1444239	59192.66469				PQ Gem	1
TMTS J08382201+4838023	58907.51608				EI UMa	1
TMTS J21334362+5107248	59835.54625				1RXS J2133+51	1
TMTS J22165027+4646412	59822.49572			E	HBHA 4705-03	8
Nova-like variables						
TMTS J01385585+2429393	59931.42144				SDSS J0138+24	9
TMTS J05064797+8319233	59155.69393	$85.8 \pm 0.3$	0.327	E	V1024 Cep	1
TMTS J05572400+7241528	59597.42662	$188.40 \pm 2.08$	0.265	L	LS Cam	1
TMTS J06293373+7104361	59597.42655				BZ Cam	1
TMTS J07565314+0858318	59636.46295	$95.0 \pm 0.4$	0.300	E	SDSS J0756+08	10
TMTS J08021533+4010463	58863.60606	$55.8 \pm 0.5$	0.090	L	SDSS J0802+40	1
TMTS J08125687+1911572	59640.46993			E	NS Cnc	1
TMTS J08223605+5105242	59182.64784			E	BH Lyn	1
TMTS J09030895+4117467	58941.48244				BP Lyn	1
TMTS J09201115+3356421	59207.67148	$110.3 \pm 0.4$	0.125	L	BK Lyn	1
TMTS J10481806+5218295	59665.50191	$191.52 \pm 1.18$	0.146	L	LY UMa	1
TMTS J23400423+3017476	59846.49587	$122.4 \pm 0.2$	0.151	L	V378 Peg	1



Table 1. Cont.

Name	Start Time (MJD)	$P_{\text{pho}}$ (min)	Amplitude (mag)	Feature	VSX Name	Reference
Polars						
TMTS J00185684+3454451	59148.44826				V479 And	1
TMTS J05154141+0104402	59249.44113			E	V1309 Ori	1
TMTS J07112595+4404048	59190.65350	$118.56 \pm 0.13$	1.743	E	V808 Aur	11
TMTS J11042565+4503131	59673.50834			E	AN UMa	1
TMTS J13075377+5351303	58923.56208	$79.6 \pm 0.2$	0.681	H	EV UMa	1
Candidates						
TMTS J02461608+6217029	59529.43927	$109.7 \pm 0.4$	0.156	L	V495 Cas	new
TMTS J03394099+4148057	59544.42431	$189.5 \pm 0.7$	0.212	L	None	9
TMTS J03471387+1611083	59883.58651	$97.7 \pm 0.8$	0.262	L	MLS_J0347+16	new
TMTS J04405040+6820355	59927.66419	$110.0 \pm 1.1$	0.262	L	None	new
TMTS J06183036+5105550	59202.41861	$107.4 \pm 0.4$	0.139	L	None	12
TMTS J07200739+4516113	59190.67704	$90.9 \pm 1.0$	> 1	H	MASTER OT J0720+45	13
TMTS J09011350+1447046	59209.66682	$89.57 \pm 1.31$	0.076	L	SDSS J0901+14	14

Note: Column (1), TMTS designation; column (2), the time when the TMTS observation started; column (3), photometric period corresponding to the maximum power in the LSP of the TMTS observation; column (4), peak-to-peak amplitude obtained from the best-fitting model of fourth-order Fourier series; column (5), light-curve feature defined in Section 2.2.2 (E, Eclipse; R, Rapid periodic variation; L, Low-amplitude periodic variation; H, High-amplitude periodic variation); column (6), name in VSX; column (7), reference of the corresponding source. The \* symbol indicates that the source was observed on two separate nights. References: (1) Downes et al. [38]; (2) Drake et al. [47]; (3) Osborne, J. P. et al. [48]; (4) Denisenko et al. [49]; (5) Kato et al. [50]; (6) Kozhevnikov [51]; (7) Witham et al. [52]; (8) Yakin et al. [53]; (9) Hou et al. [43]; (10) Szkody et al. [40]; (11) Thorne et al. [54]; (12) Lin et al. [31]; (13) Denisenko [46]; (14) Szkody et al. [45].

## 2.2. Light-Curve Analysis

### 2.2.1. Periodic Variations

We searched for periodic variations in the TMTS light curves using the Lomb–Scargle periodogram (LSP; Lomb [55], Scargle [56]). The frequency range was set to  $2/T \leq f \leq f_{\text{nyq}}$ , where  $T$  is the time span of each light curve, and  $f_{\text{nyq}}$  is the Nyquist frequency, estimated as half of the average sampling rate. The method adopted to compute the LSP for the TMTS light curves was already described in detail by Lin et al. [31]. The false-alarm probability (FAP) was estimated as

$$\text{FAP} = 1 - [1 - \exp(-z)]^{N_{\text{eff}}}, \quad (1)$$

where  $z$  is the LSP power, and  $N_{\text{eff}}$  is the effective number of independent frequencies.  $N_{\text{eff}}$  is approximated as  $f_{\text{nyq}}T$  [57]. We adopted a significance threshold of  $\text{FAP} = 0.001$  throughout this work.

From the TMTS LSPs of CV samples, we determined the photometric period corresponding to the maximum LSP power,  $P_{\text{pho}}$ , if the maximum LSP power was higher than the threshold (see Table 1). Then, we used a compound model of fourth-order Fourier series with a period equal to  $P_{\text{pho}}$  plus a second-order polynomial to fit all TMTS light curves (see Equation (7) of Lin et al. [31]). The peak-to-peak amplitudes obtained from the fourth-order Fourier series are listed in Table 1.

### 2.2.2. Light-Curve Features

With the minute-cadence photometry from TMTS, we can characterize the uninterrupted light curves of these CVs. Here, all short-timescale light-curve features were classified into four distinguishable types, as follows.

- **Eclipse.** Thanks to densely sampled photometry, the TMTS light curves allow us to characterize the detailed profiles of eclipses for the eclipsing CVs. In our CV samples, the eclipse depth ranges from a few tenths of magnitude to more than 2.0 mag. The

emergence of an eclipse provides direct evidence supporting the notion that the CV system has an orbital inclination approaching  $90^\circ$ .

- **Low-amplitude periodic variation.** With the amplitude distribution of noneclipse CV systems (see Figure 1), 20 CV samples presented periodic modulation amplitude of about 0.1–0.4 mag, while 2 CV samples exhibited a significantly higher modulation amplitude. Low-amplitude periodic variations here are defined as periodic variations with an amplitude lower than 0.4 mag, which are typically caused by the hump/superhump of CVs and are thus tightly related to their orbital periods.
- **High-amplitude periodic variation.** In contrast, high-amplitude periodic variations represent modulations with an abnormally high amplitude. Here, we roughly define them as periodic variations with an amplitude larger than 0.4 mag.
- **Rapid periodic variation.** Since the quasi-periodic oscillations of DNe and rotation modulations of IPs are difficult to distinguish with the single-night light curves, here, the rapid periodic variations represent all periodic or quasi-periodic variations below 20 min, significantly shorter than the periodic variations induced via orbital modulations.

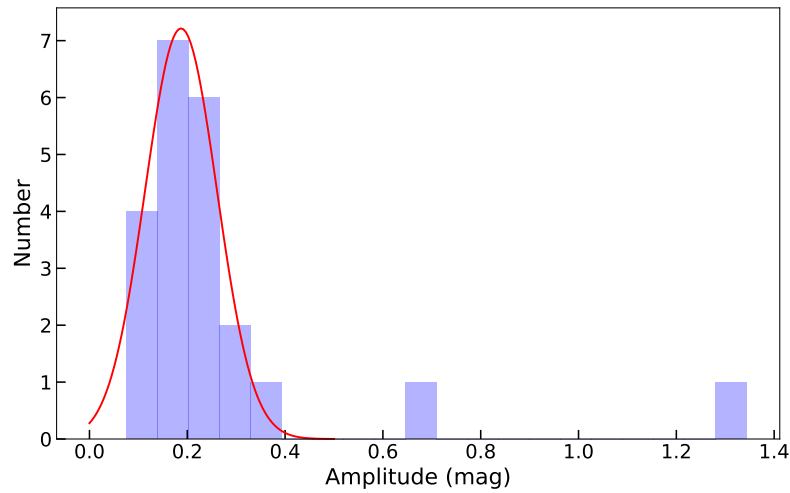


**Figure 1.** Distribution of the amplitude of periodic variations from noneclipse CVs. The red line represents a Gaussian fit.

### 2.3. Spectroscopic Analysis

With the spectra collected from LAMOST, LST, and XLT, we further performed a spectroscopic study of our CV samples. (Note that the CV candidates are not included in this study.) We selected those CVs with better determinations of subtypes and orbital periods from our 64 CV samples, excluding 7 candidates and 3 sources without an orbital period. Only spectra with a signal-to-noise ratio (SNR)  $> 10$  and variation coefficient (VC)  $< 1$  are included in our analysis, where VC is defined as the ratio of the standard deviation to the mean value of the SNR. VC is used to evaluate the quality of the spectrum, which is acceptable when  $VC < 1$  [58]. In addition, only those spectra showing emission features were included in the analysis since we are interested in the emitting process in the CVs. Finally, 44 CVs were included in the spectroscopic analysis.

The equivalent width (EW) of  $H\alpha$  emission,  $EW_{H\alpha}$ , was calculated by integrating the flux excesses above the continuum:

$$EW = \int \frac{F_\lambda - F_c}{F_c} d\lambda, \quad (2)$$

where  $F_\lambda$  represents the emission flux at wavelength  $\lambda$ , and  $F_c$  denotes the continuum flux.  $F_\lambda$  is the flux in the wavelength range of 6480–6640 Å. Such a wide range can include the entire broadened profile of  $H\alpha$  emission. The continuum flux was obtained by linearly fitting the spectral ranges 6480–6510 Å and 6620–6640 Å, and no emission component

emerged over these ranges in our spectra. Additionally, the full width at half-maximum intensity (FWHM) is the wavelength interval between halves of the maximum flux in the emission lines.

We used Monte Carlo simulations to estimate the uncertainties of  $EW_{H\alpha}$  and  $FWHM_{H\alpha}$ . The flux of the spectra was randomly sampled according to the uncertainty at each wavelength. After repeating the simulation 100 times, the standard deviations of the measured  $EW_{H\alpha}$  and  $FWHM_{H\alpha}$  were taken as the corresponding uncertainties. The typical uncertainties for the two quantities are both  $\sim 1 \text{ \AA}$ .

### 3. Individual Systems

The minute-cadence observations from TMTS enabled us to study the short-timescale light variations of all these CV samples, including the newly discovered ones (see Table 1). In particular, the TMTS data reveal new photometric periods for some known CVs, together with the observations from *TESS* and the Zwicky Transient Facility (ZTF; Bellm et al. [59], Masci et al. [60]).

#### 3.1. Newly Discovered CVs and CV Candidates

##### 3.1.1. TMTS J04405040+6820355

TMTS J04405040+6820355 (hereafter J0440) shows a significant light-variation period of  $P_1 = 110.0 \pm 1.1 \text{ min}$  in the TMTS light curve obtained on 14 December 2022 (UTC dates are used throughout this paper); see Figure 2. Broad  $H\alpha$  emission is superimposed on a blue continuum in the spectrum obtained with the Xinglong 2.16 m telescope on 2 October 2023 (Figure 2). Given the location of J0440 in the Gaia color-magnitude diagram ( $M_{\text{abs,G}} = 5.4 \text{ mag}$  and  $G_{\text{BP-RP}} = 0.13 \text{ mag}$ ), we infer that J0440 is a new CV candidate (see also Lin et al. [35]).

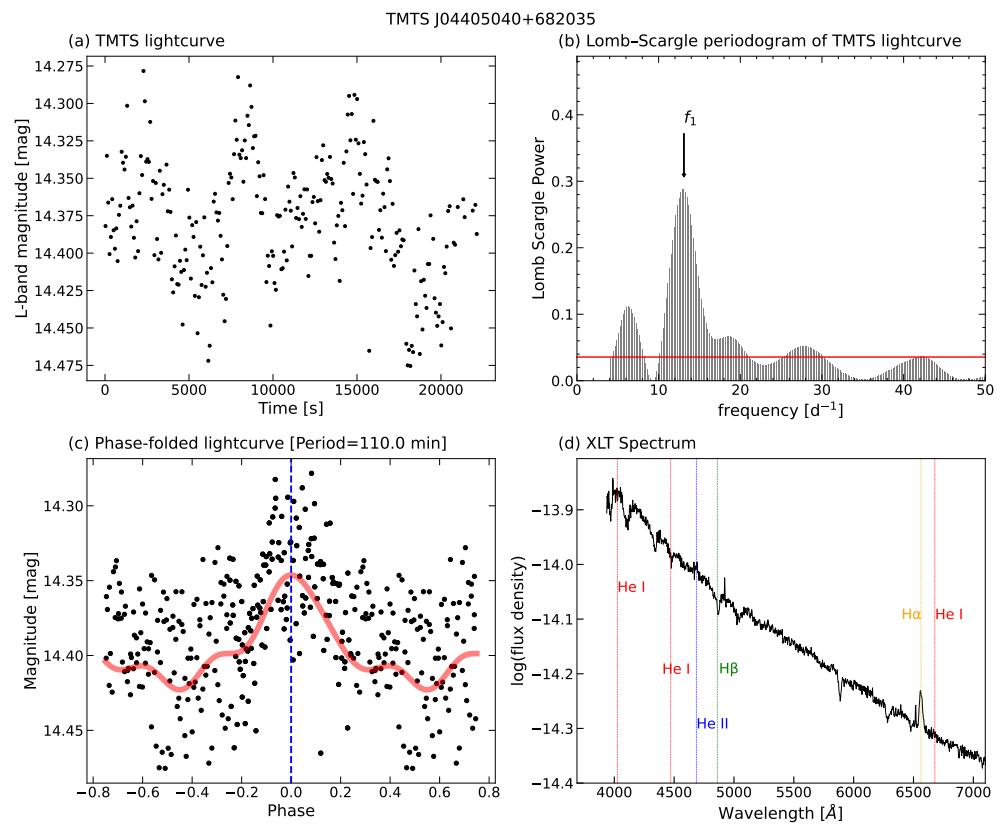


**Figure 2.** (a) TMTS light curve of TMTS J04405040+6820355; (b) Lomb–Scargle periodogram of TMTS J04405040+6820355; (c) phase-folded TMTS light curve with  $P_1 = 110.0 \text{ min}$ , with the red line representing the best-fit model of fourth-order Fourier series; (d) the XLT spectrum of TMTS J04405040+6820355.

The five-year light curves provided via ZTF failed to reveal any outburst for this source; along with the presence of  $H\beta$  absorption, this implies that it might be an NL with an optically thick disk.

### 3.1.2. TMTS J06183036+5105550

TMTS J06183036+5105550 (hereafter J0618) is a new CV discovered via TMTS and reported in the catalog of TMTS short-period variable stars [35]. Its spectrum shows a faint He II emission line around 4686 Å. According to the *Swift*/XRT observation conducted on 29 October 2022, this source has an X-ray luminosity of  $\sim 10^{31}$  erg s<sup>-1</sup>. Two periodicities,  $P_1 = 107.4 \pm 0.4$  min and  $P_2 = 11.165 \pm 0.004$  min, are revealed via the TMTS light curve. These clues favor the classification of this object as an intermediate polar candidate.

We further explored the properties of this source by conducting a polarization observation on 22 November 2022 with the Kast double spectrograph on the Shane 3 m telescope at Lick Observatory, USA. The spectropolarimetric results are shown in Figure 3, where  $q = Q/I$  and  $u = U/I$  are the normalized Stokes parameters.  $Q$  and  $U$  describe the differences of fluxes when the electric vector oscillates in two perpendicular directions, and  $I$  is the total flux. The observed polarization,  $p$ , is calculated as  $p_{\text{obs}} = \sqrt{q^2 + u^2}$ , and the polarization angle is calculated through  $\text{PA}_{\text{obs}} = (1/2) \arctan(u/q)$ . Since electromagnetic waves passing through interstellar dust will become polarized, the galactic interstellar polarization (ISP) is also taken into account when computing the intrinsic polarization from the CV system. Following the procedure described by Patra et al. [61], the ISP of J0618 was removed by subtracting the observed polarization from the intrinsically unpolarized star within the 1° of this object.

As seen in Figure 3, a linear polarization of  $\sim 0.6\%$  was detected for J0618, comparable to the 0.8% linear polarization reported for intermediate polar RE 0751+14 in the  $R$  band [62]. The values of the polarization angle are noisy for some points, but in general, they are not randomly scattered. In the case of magnetic CVs, material from the companion star is accreted onto the magnetic poles of the WD, leading to cyclotron radiation [63]. The higher harmonics of the fundamental frequency will generate linear polarization [7]. Unlike polars, polarized light from IPs will be diluted due to the emission from the accretion disk, WD, and so on. This leads to the fact that polarized emission is detected only in a few IP systems [64]. With all the above observational evidence, we suggest that J0618 is an intermediate polar.

## 3.2. New Light-Variation Features from Known CVs

### 3.2.1. SDSS J013855.86+242939.2

SDSS J013855.86+242939.2 (TMTS J01385585+2429393, hereafter J0138) is a relatively poorly studied CV identified by cross-matching SDSS WD candidates with LAMOST spectra [65]. Hou et al. [43] classified it as a magnetic CV according to the comparable strength of  $H\beta$  and He II  $\lambda 4686$  lines. Nevertheless, they also emphasized that this classification was based only on the characteristic lines and may not be accurate. From ZTF  $r$ -band observations, the brightness of this CV can change from  $\sim 15$  mag to  $\sim 18$  mag. The brightness variation of this CV resembles that of magnetic CVs [66,67].

During the TMTS observations, this source is at its high-luminosity state, with the TMTS  $L$ -band magnitude being  $\sim 15.4$  mag. As shown in Figure 4, some flickering can be seen in its phase-folded light curve. A new photometric period,  $P_1 = 179.0 \pm 2.3$  min, was revealed via the LSP. If the period is its orbital period, J0138 is a CV located at the period-gap boundary. However, the *TESS* observations of this object (TIC 353851691) did not detect any significant periodic signal above 2 day<sup>-1</sup>, while the ZTF  $r$ -band and  $g$ -band LSP only present some daily aliases. Hence, the physical origin of this photometric period needs further observations and analysis.

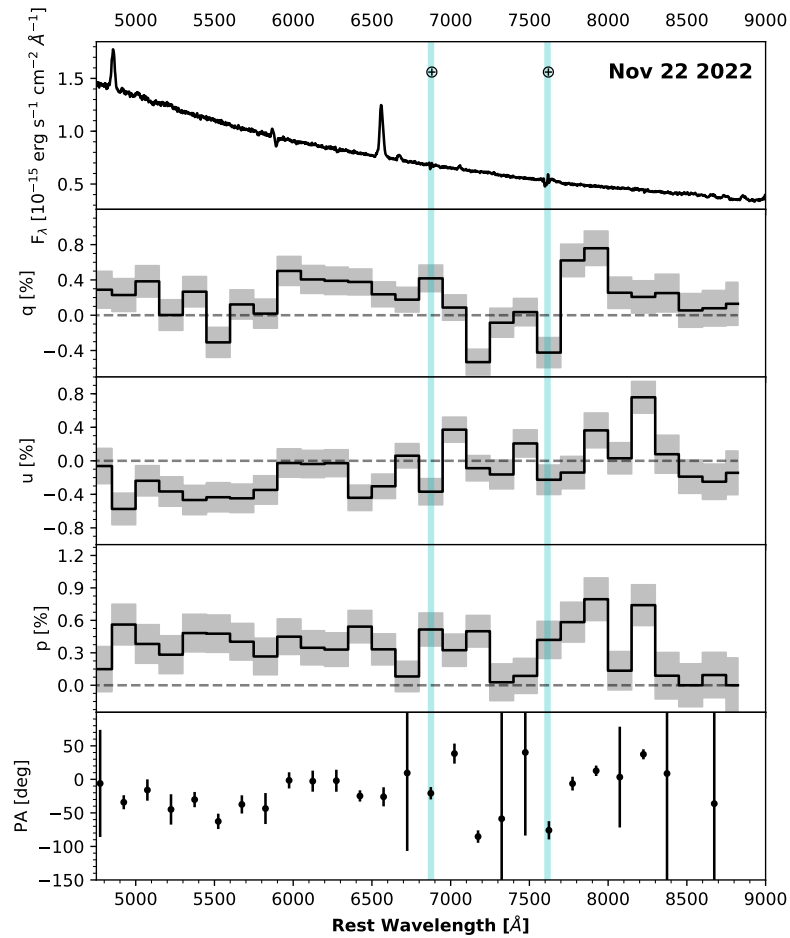


**Figure 3.** Spectropolarimetry of TMTS J06183036+5105550 obtained with the Lick/Shane 3 m telescope on 22 November 2022. The cyan vertical bands represent the regions of telluric correction. The top panel presents the total-flux spectrum. The panels below the total-flux spectrum represent the polarimetry after the ISP correction. The gray-shaded area indicates the associated  $1\sigma$  uncertainty.

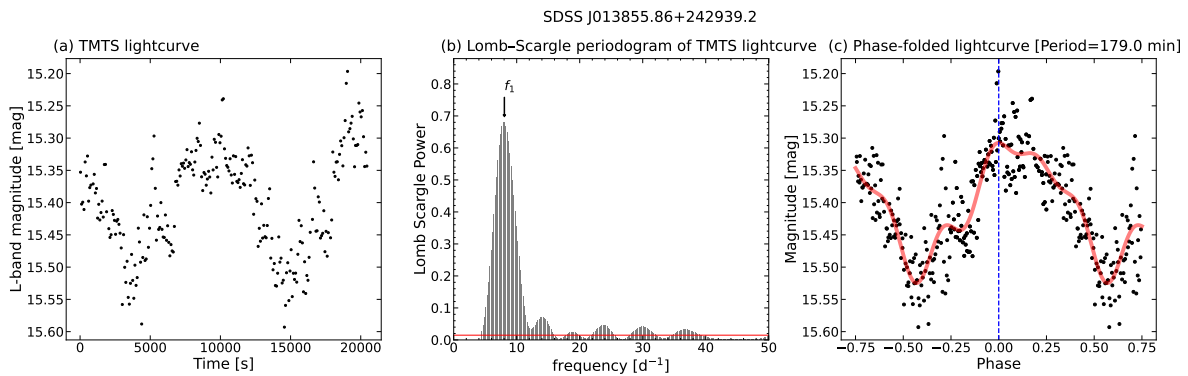


**Figure 4.** (a) TMTS light curve of SDSS J013855.86+242939.2; (b) Lomb–Scargle periodogram of SDSS J013855.86+242939.2; (c) phase-folded light curve with a period of 179.0 min. The red line represents the best-fit model of fourth-order Fourier series.

### 3.2.2. TMTS J03471387+1611083

TMTS J03471387+1611083 (also LAMOST J034713.84+161108.2, hereafter J0347) was first classified as an RR Lyrae star in the Catalina Survey [68], and then it was identified as a CV candidate with LAMOST spectroscopic observations [69]. Following the instructions from [35], the Gaia absolute magnitude  $M_{\text{abs,G}} = 6.22$  mag and dereddened

$G_{\text{BP-RP}} = 0.11$  mag support that J0347 is a CV, rather than an RR Lyrae variable. The TMTS light curve reveals a periodically occurring hump feature, which could be caused by a bright spot on the accretion disk. The TMTS LSP (bottom-left panel of Figure 5) presents two periodic signals, namely  $P_1 = 97.7 \pm 0.8$  min and  $P_2 = 155.0 \pm 2.1$  min. For comparison, we also checked the light curve of J0347 from *TESS* observations and computed the corresponding LSP (see the left panels of Figure 5). Two periodic signals,  $P_3 = 101.064 \pm 0.004$  min and  $P_4 = 2.444 \pm 0.003$  days, were also revealed from the *TESS* LSP (middle-right panel of Figure 5). Without an accurate determination of the orbital period, the origin of  $P_1$  and  $P_3$  could not be determined reliably; a further study of J0347 is expected.

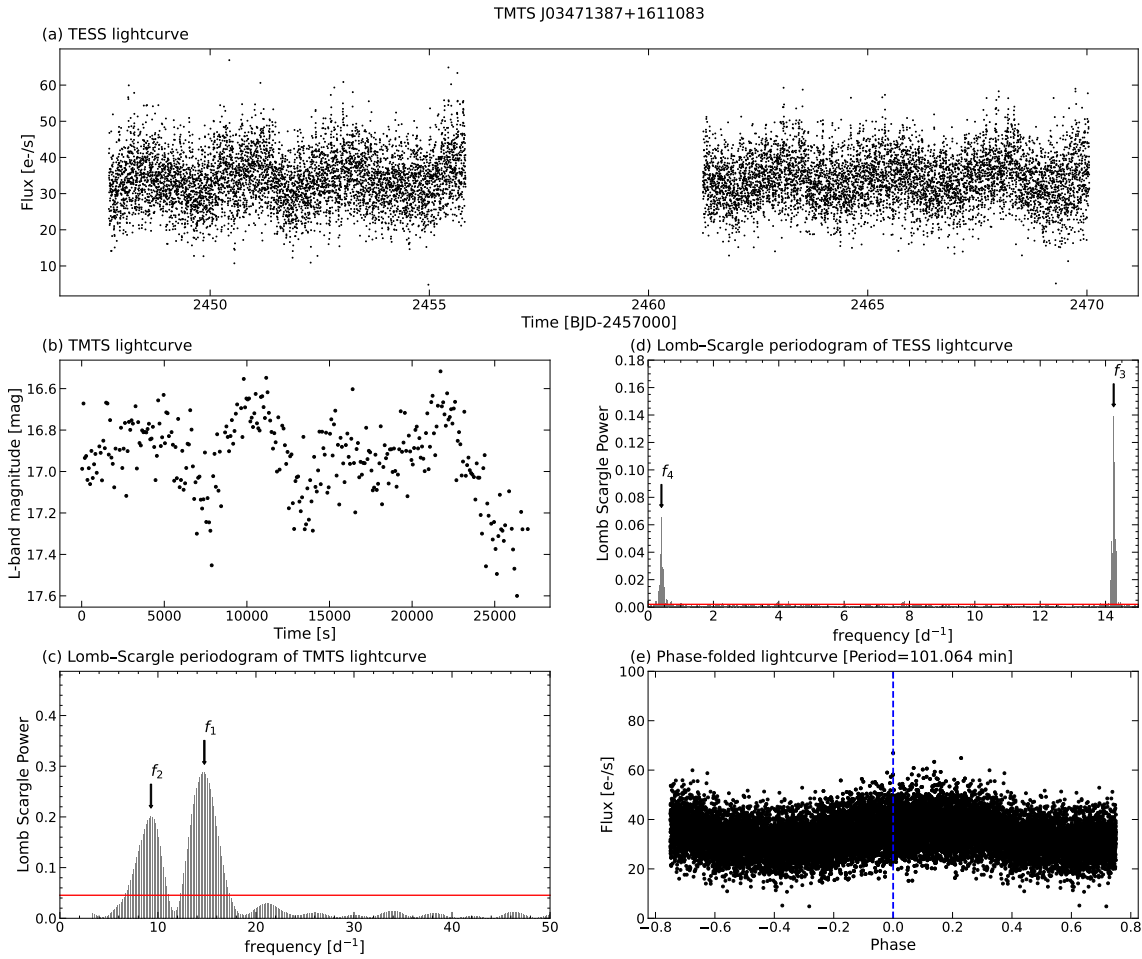


**Figure 5.** (a) *TESS* light curve of TMTS J03471387+1611083; (b) TMTS light curve of TMTS J03471387+1611083; (c) Lomb–Scargle periodogram of the TMTS light curve in (b); (d) Lomb–Scargle periodogram of the *TESS* light curve in (a); (e) phase-folded light curve with  $P_3 = 101.064$  min.

### 3.2.3. FO Per

TMTS J04083502+5114484 (FO Per) was first discovered by Morgenroth [70], and then classified as a DN with spectroscopic observations [71]. Sheets et al. [72] determined its orbital period as 211.2 min or 247.8 min by measuring the radial velocities of H $\alpha$  emission. Sheets et al. [72] suggested a 4.13 hr orbital period since the period is consistent with those of nova-like variables. However, this estimate is not conclusive, as the orbital periods of many DNe also fall into this range.

In the periodograms shown in Figure 6, a photometric period of  $P_1 = 208.0 \pm 1.4$  min is detected from the TMTS observation, while another period  $P_2 = 202.517 \pm 0.002$  min is detected from the *TESS* observation. Both photometric periods roughly agree with the



presence of a shorter orbital period suggested by Sheets et al. [72], implying that the orbital period of FO Per is more likely 211.2 min.

From the ZTF *r*-band light curve, the brightness of TMTS J04083502+5114484 can vary from 13.5 mag to 17 mag. The ZTF light curve also indicates that FO Per was going into outburst during the TMTS observation, and this CV system then reached  $\sim 13.5$  mag ten days later. It is worth noting that the light-variation amplitude of this DN can reach  $\sim 1.5$  mag, much larger than that of other DNe in our samples, and thus, it is possibly caused by a different physical process.

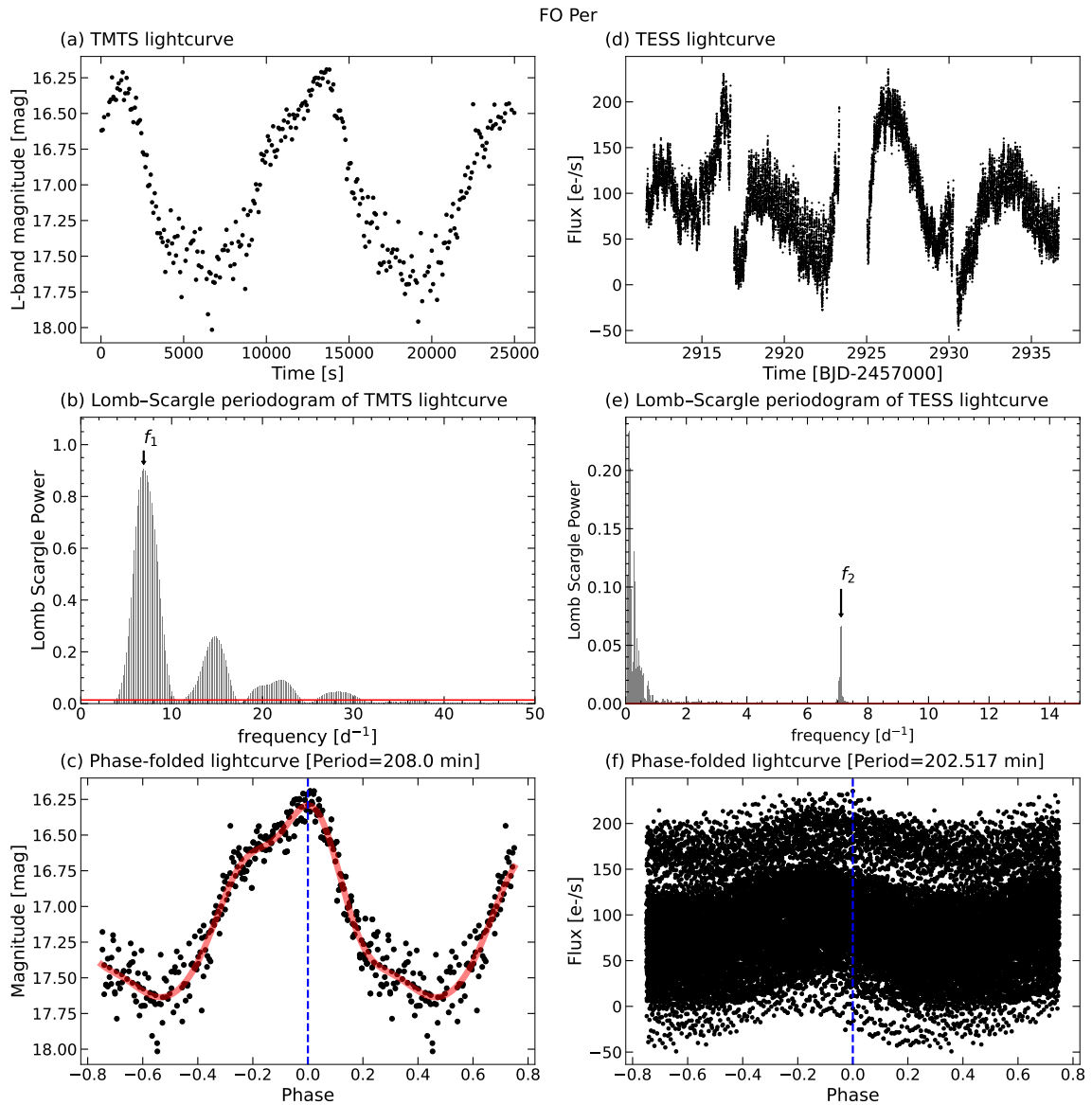


**Figure 6.** (a) TMTS light curve of FO Per; (b) Lomb–Scargle periodogram of the TMTS light curve; (c) phase-folded TMTS light curve with  $P_1 = 208.0$  min, with the red line representing the best-fit model of fourth-order Fourier series; (d) *TESS* light curve of FO Per; (e) Lomb–Scargle periodogram of the *TESS* light curve in (d); (f) phase-folded *TESS* light curve with  $P_2 = 202.517$  min.

### 3.2.4. SS Aur

TMTS J06132238+4744248 (SS Aur) is a DN with an orbital period of  $262.23 \pm 0.15$  min derived from radial velocities [73–75]. Two periods can be resolved in the periodogram of its TMTS light curve, namely  $P_1 = 108.535 \pm 0.015$  min and  $P_2 = 255.83 \pm 0.08$  min (see

Figure 7). Among these two periods,  $P_2$  is likely a negative superhump. If so, the period excess is  $\epsilon = -0.024$ , consistent with the relation between period excess and negative superhump period given by Bruch [13].

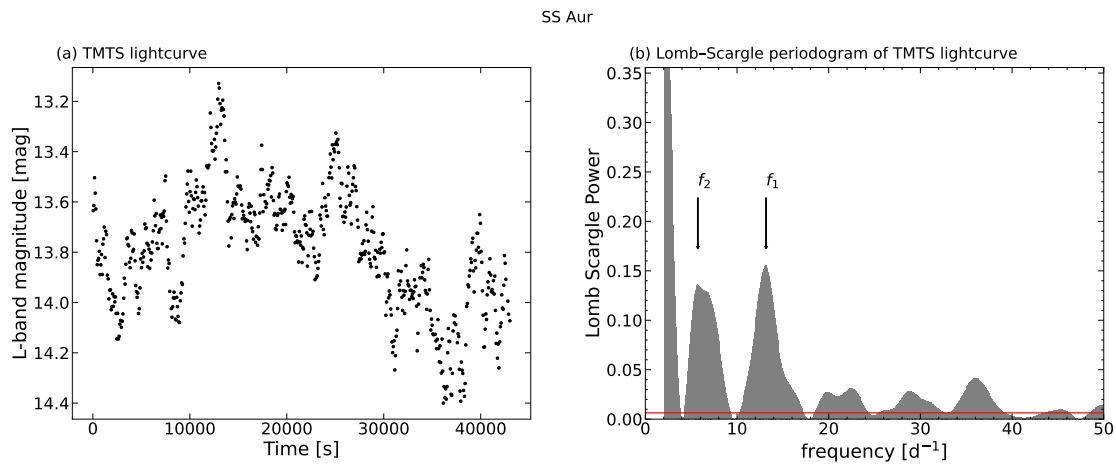


**Figure 7.** (a) TMTS light curve of SS Aur; (b) Lomb–Scargle periodogram of the TMTS light curve.

### 3.2.5. V378 Peg

TMTS J23400423+3017476 (V378 Peg) is an NL that was discovered by the Palomar–Green survey [76] and first classified as a CV by Koen and Orosz [77]. The orbital period of V378 Peg derived from radial velocities is  $P_{\text{orb}} = 199.55 \pm 0.06$  min [78]. Negative superhumps ( $\sim 3.2$  h) of V378 Peg were detected by both Ringwald et al. [78] and Kozhevnikov [79]. From our TMTS light curve, we detected a period of  $P_1 = 122.4 \pm 0.2$  min, which is shown in Figure 8. Following VanderPlas [57], we calculated the LSP of a window function of the TMTS light curve, but we did not find any fake spikes at the location of  $P_1$ . This period is unlikely to be a superhump, owing to the large difference with  $P_{\text{orb}}$ . Although we do not exactly know its physical origin, it reflects the complexity of disk oscillations in CVs.

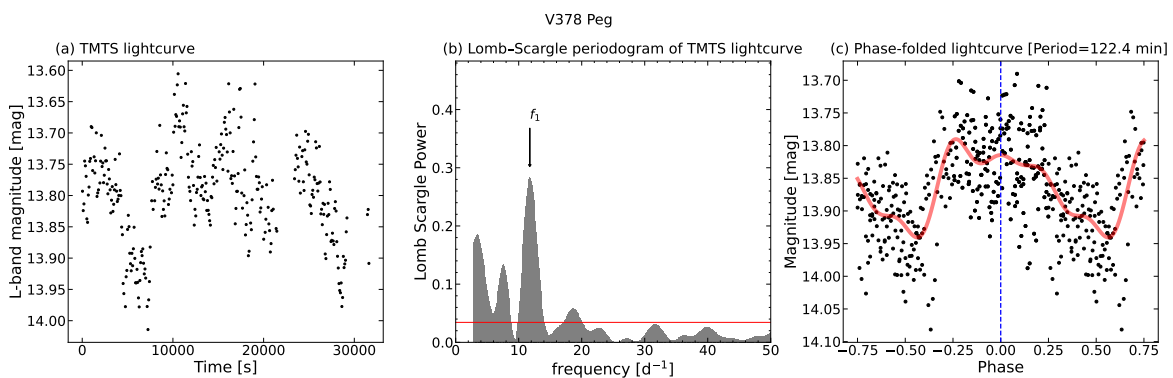


**Figure 8.** (a) TMTS light curve of V378 Peg; (b) Lomb–Scargle periodogram of the TMTS light curve; (c) phase-folded TMTS light curve with  $P_1 = 122.4$  min (a second-order polynomial was subtracted to detrend), with the red line representing the best-fit model of fourth-order Fourier series.

### 3.2.6. Possible QPOs

DNe sometimes exhibit quasi-periodic fluctuations with a period ranging from a few tens to a few thousands of seconds [80]. Among them, the rapid oscillations, with a timescale of a few dozen seconds, are called dwarf nova oscillations (DNOs), while the oscillations with a longer period ranging from a few hundred to a few thousand seconds are regarded as quasi-periodic oscillations (QPOs). Owing to timing resolution, TMTS cannot detect any DNOs; instead, some possible QPOs were detected from the uninterrupted light curves of TMTS.

TMTS J01043552+4117576 (RX And) is a Z Cam-type DN with an orbital period of 5.08 h [81]. A periodicity of 35.7 s (DNO) was found in previous light curves [82], while Warner et al. [83] proposed that there was weak evidence of a 1000 s oscillation. In the upper panel of Figure 9, the LSP of the TMTS observations presents a period signal  $P_1 = 20.285 \pm 0.006$  min, within the typical timescale of QPOs.

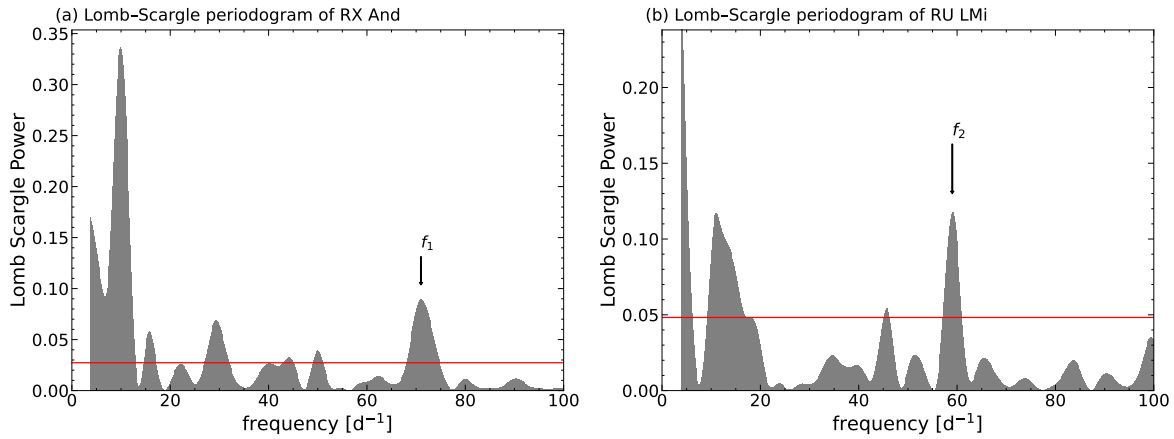


**Figure 9.** (a) Lomb–Scargle periodogram of RX And; (b) Lomb–Scargle periodogram of RU LMi.

TMTS J10020745+3351005 (RU LMi) was initially identified as a CV by Wagner et al. [84]. With photometric observations, Howell et al. [85] reported an orbital period of 355 min, while the spectrum of this object was consistent with those of typical DNs [86]. In the lower panel of Figure 9, a period signal of  $P_2 = 24.40 \pm 0.07$  min was detected via TMTS, which is also within the typical timescale of QPOs.

#### 4. Discussion

##### 4.1. Statistical Properties of EW and FWHM for Nonmagnetic CVs

As introduced in Section 2.3, we collected the spectra of 44 CVs, for which the EW and FWHM of  $H\alpha$  emission were measured. Since the accretion in magnetic CVs is governed by magnetic fields, their accretion geometries are essentially different from those of non-magnetic systems in which the radiation of accretion disks dominates the emission [10,87]. Here, we focus on the spectroscopic properties of the 28 nonmagnetic CVs.

According to the period gap [18], the CVs can be divided into two groups: short-period CVs with  $P_{\text{orb}} < 2.15$  h and long-period CVs with  $P_{\text{orb}} > 3.18$  h. Adopting the orbital periods provided from the VSX shows that the 28 nonmagnetic CVs consist of 19 long-period systems (10 DNe and 9 NLs) and 9 short-period ones (9 DNe).

Because the sample of nonmagnetic CVs from the TMTS observations is relatively small, spectral data from the SDSS were also included in double-checking the robustness of the distribution trend. The SDSS CVs were cross-matched with the VSX catalog to collect their identification information, such as the subtype and orbital period. Then, the SDSS spectra of those nonmagnetic CVs (DNe and NLs) were analyzed with the same criteria as described in Section 2.3.

The spectra of DNe in the outburst state usually show narrow Balmer emission lines superposed on broad absorption wings. We adopted a composite model, a positive Gaussian function for the emission feature plus a negative one for the absorption, to fit such a profile. We found that the emission components during the outburst tend to have a small EW (typically,  $EW_{H\alpha} < 10$  Å). For example, the  $EW_{H\alpha}$  of SDSS J105550.08+095620.4 is 8.54 Å during the outburst, while its  $EW_{H\alpha}$  was reported to be 70 Å in quiescence [88]. The significant difference in EW between the outburst and quiescent states prevented us from performing a reasonable comparison of the emission strengths of DNe. We thus excluded the DNe in the outburst state from our statistical study.

For the TMTS sample, the distributions of  $EW_{H\alpha}$  are shown in Figure 10, in which the nonmagnetic CVs with shorter orbital periods tend to have a wider feasible range of  $EW_{H\alpha}$  than those with longer periods. The mean  $EW_{H\alpha}$  values of CVs in the two subclasses are 125 Å and 26 Å, respectively. A similar trend can be seen from the  $FWHM_{H\alpha}$  distributions (see the blue columns in Figure 11).

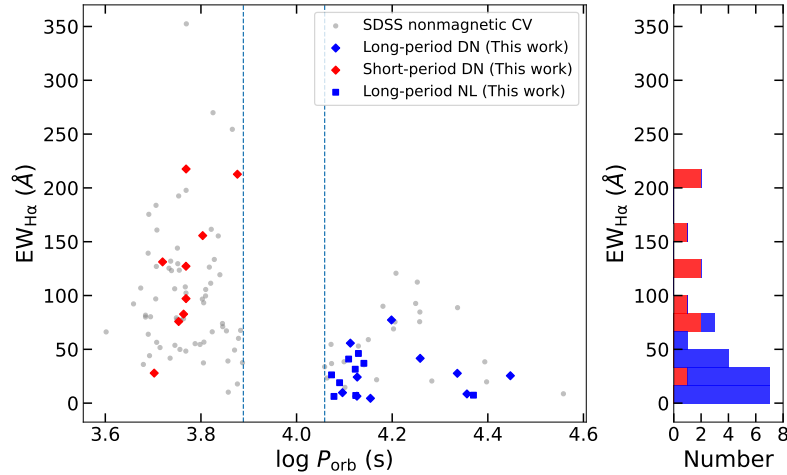


**Figure 10.** Distribution of  $EW_{H\alpha}$  measured for the nonmagnetic CV sample as a function of  $\log P_{orb}$ . Diamond and square points represent the DNe and NLs in this catalog, respectively, while red and blue colors indicate short-period and long-period subclasses. Gray circle points represent the sources from Szkody et al. [40]. The two vertical blue dashed lines mark the period gap ( $2.15 \text{ h} \lesssim P_{orb} \lesssim 3.18 \text{ h}$ ; see Knigge [18]).

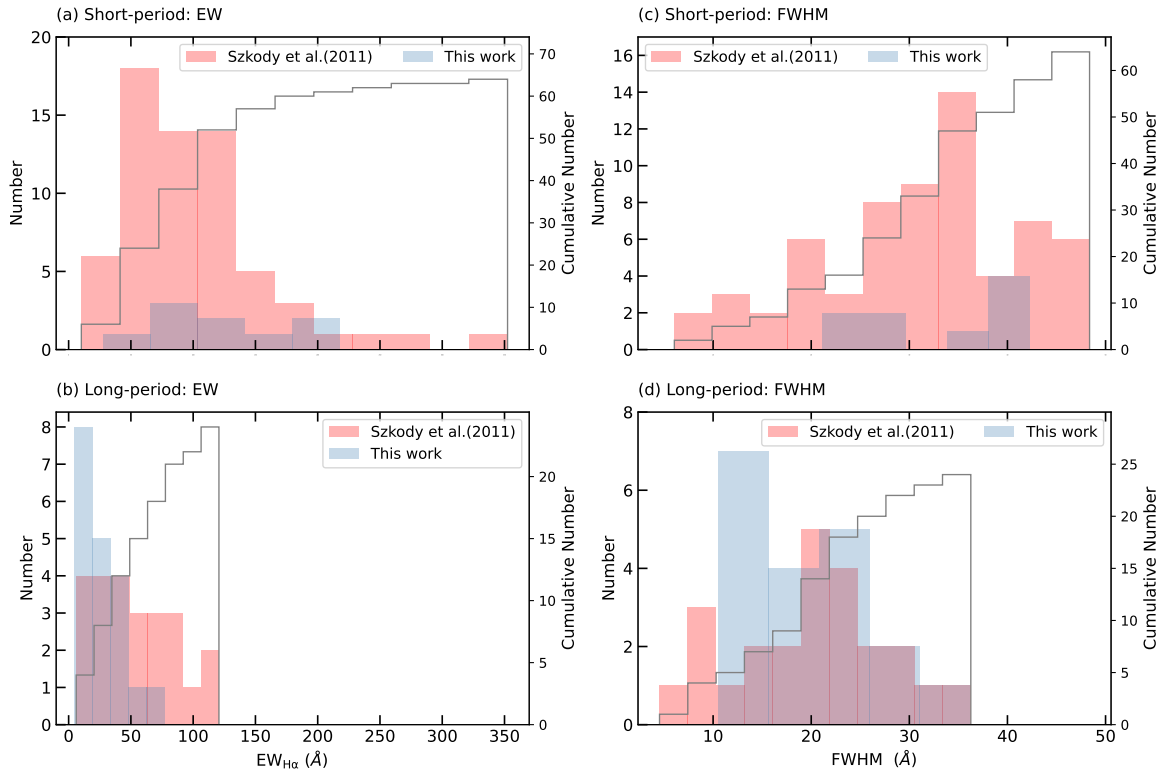


**Figure 11.** Histogram distribution of EW (a,b) and FWHM (c,d) of  $H\alpha$  emission in spectra of nonmagnetic CVs. Panels (a,c): distribution of short-period nonmagnetic CVs. Panels (b,d): distribution of long-period nonmagnetic CVs. The red columns represent the nonmagnetic CVs from Szkody et al. [40], while the blue columns represent the nonmagnetic CVs from our sample. The gray lines show the cumulative distributions of the SDSS nonmagnetic CV sample.

The EW/FWHM distributions for 64 short-period CVs and 24 long-period CVs obtained from SDSS observations are appended to Figure 11 (the red columns; see also Table 2). The distribution trend yielded from the SDSS spectra is consistent with that revealed in the TMTS CV samples. To quantify the difference in  $H\alpha$  strength between the long-period and short-period nonmagnetic CVs, we performed the two-sample Kolmogorov–Smirnov test (K-S test) for the SDSS  $EW_{H\alpha}$  distributions and obtained a  $p$ -value of 0.003, suggesting that the  $EW_{H\alpha}$  distributions above/below the period gap are quite different. Similarly, the  $p$ -value obtained for the SDSS  $FWHM_{H\alpha}$  distribution is 0.00005.

**Table 2.** Summary of the statistics of the distributions for the short-period and long-period nonmagnetic CVs from our sample and Szkody et al. [40]. The subscripts “mean” and “std” respectively represent the mean values and standard deviations of EW/FWHM for short-period and long-period classes.

Class	$EW_{\text{mean}}$ ( $\text{\AA}$ )	$EW_{\text{std}}$ ( $\text{\AA}$ )	$FWHM_{\text{mean}}$ ( $\text{\AA}$ )	$FWHM_{\text{std}}$ ( $\text{\AA}$ )
Short-period (Szkody et al. [40])	101.19	60.86	30.96	10.16
Long-period (Szkody et al. [40])	53.07	32.70	19.90	8.07
Short-period (this work)	125.33	59.30	33.55	7.26
Long-period (this work)	26.47	19.33	19.47	6.96

As shown in Figure 11, the EW and FWHM of the short-period nonmagnetic CVs are systematically larger than those of long-period systems. In particular, Figure 10 demonstrates that only short-period systems exhibit large  $EW_{H\alpha}$  (e.g.,  $\gtrsim 130 \text{\AA}$ ) in their spectra. We supposed that the accretion disks in short-period nonmagnetic CVs tend to have smaller radii, which means that the  $H\alpha$  emission regions are potentially closer to the accretors and thus suffer from a more intense Kepler broadening. In Figure 10, the  $H\alpha$  strength among long-period sources does not show a correlation with  $P_{\text{orb}}$ , which is a clue to the possible transformation of the accretion process that occurs when CVs go through the period gap.

Although the evolutionary path of CVs has been well understood [89], there are still some challenges in interpreting the large spread of CV orbital period distribution and the presence of more massive WDs in CVs [90,91]. These facts suggest that our understanding of CV evolution is incomplete. The distributions of  $H\alpha$  strength presented here shed light on the CV evolution.

Since nonmagnetic CVs in the TMTS CV samples present the same  $EW_{H\alpha}$  and  $FWHM_{H\alpha}$  tendency as those from the SDSS sample, the effect of selection bias on the above conclusion is unlikely to be significant. Note that the SDSS CV sample should be more homogeneous since it includes faint sources and covers a wide color range [92,93]. However, the statistical conclusions in this work will require further verification with a more complete sample in the future.

#### 4.2. The Implications of TMTS Light Curves

In Section 2.2.2, we highlighted several CV samples showing abnormally large-amplitude periodic variations. The polar EV UMa exhibits a large-amplitude orbital modulation, which can be explained by a heavily beamed cyclotron emission from the accretion column. The change in the angle between the line of sight and magnetic polar within an orbital period leads to large-amplitude photometric variations in the light curves [94,95]. Differing from most DNe in our samples, the dwarf nova FO Per presents a large-amplitude orbital modulation comparable to the polars.

Since the periodic variations could be related to the specific accretion state of CVs (e.g., pre-outburst state), the high-cadence survey observations are crucial to uninterruptedly record the light variations corresponding to the short-duration states in CVs (e.g., state transition). Furthermore, the high-cadence observations from TMTS can easily capture the rapid periodic variations (i.e., spin modulations) from IPs. For example, two spin frequencies for V1033 Cas ( $P_{\text{pho}} = 9.372 \pm 0.005 \text{ min}$ ) and MU Cam ( $P_{\text{pho}} = 19.785 \pm 0.009 \text{ min}$ ) were also revealed through the TMTS data (see Figure 12).

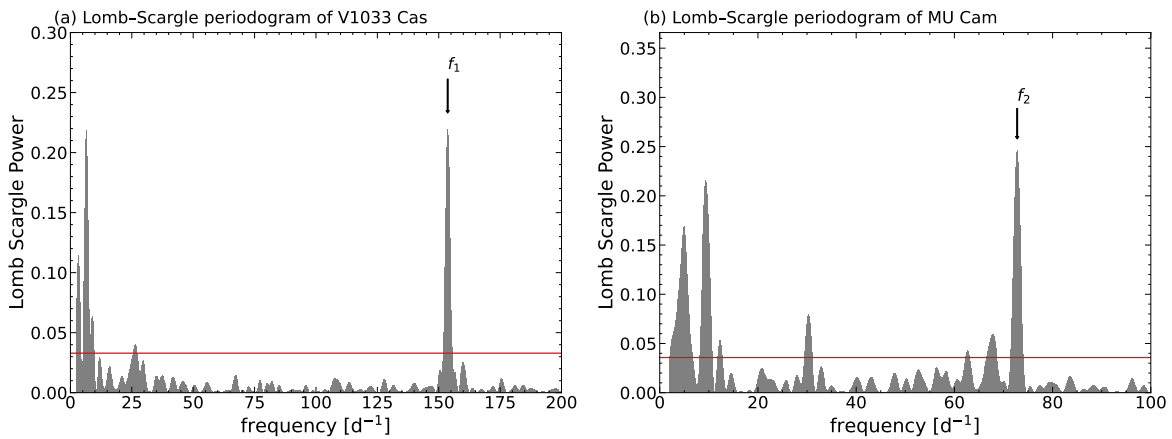


**Figure 12.** (a) Lomb–Scargle periodogram of V1033 Cas; (b) Lomb–Scargle periodogram of MU Cam;  $f_1$  and  $f_2$  indicate the spin frequencies of the two sources, respectively.

## 5. Conclusions

We have presented well-sampled light curves and spectra of 64 CVs or CV candidates observed/discovered during the first 3 years of the TMTS survey. By performing periodogram analysis, we identified two new CV candidates (TMTS J04405040+6820355 and TMTS J06183036

+5105550) and nine new photometric periods for seven known CVs from the TMTS light curves. The properties of the two new CVs and the physical origins of new periods were discussed. TMTS J04405040+6820355 is inferred to be a new DN candidate, while TMTS J06183036+5105550 could be a new IP, as indicated by a linear polarization of  $\sim 0.6\%$ .

The short-timescale features from our high-cadence light curves can be classified into four types: eclipse, low-amplitude periodic variation, high-amplitude periodic variation, and rapid periodic variation. We attempted to explore the various short-timescale variations in CVs with these features.

With the CV spectra from LAMOST, XLT, and SDSS, we found that there are significant differences in the distribution of  $H\alpha$  emissions (i.e.,  $EW_{H\alpha}$  and  $FWHM_{H\alpha}$ ) between nonmagnetic CVs located above and below the period gap, implying that the accretion nature of CVs should be tightly related to their evolutionary stages.

**Author Contributions:** Conceptualization and methodology, Q.L., J.L. (Jie Lin), and X.W.; data analysis, Q.L.; resources, Y.S., G.X., J.M., J.L. (Jialian Liu), S.Y., A.V.F., T.G.B., Y.Y., K.C.P., Y.C., Z.C., L.C., F.G., X.J., G.L., W.L. (Wenxiong Li), W.L. (Weili Lin), C.M., X.M., H.P., Q.X., D.X., and J.Z.; writing—original draft preparation, Q.L.; writing—review and editing, J.L. (Jie Lin), X.W., Z.D., and A.V.F. All authors have read and agreed to the published version of the manuscript.

**Funding:** This work was supported by the National Natural Science Foundation of China (NSFC grants 12288102 and 12033003), the Ma Huateng Foundation, and the New Cornerstone Science Foundation through the XPLOER PRIZE. J.L. is supported by the Cyrus Chun Ying Tang Foundations. A.V.F.’s team at U.C. Berkeley received support from the Christopher R. Redlich Fund, Gary and Cynthia Bengier, Clark and Sharon Winslow, Sanford Robertson, Alan Eustace, Briggs and Kathleen Wood, and many other donors. Y.-Z. Cai is supported by NSFC grant 12303054 and the International Centre of Supernovae, Yunnan Key Laboratory (No. 202302AN360001).

**Data Availability Statement:** The study’s catalogs are all available in this paper. The TMTS photometric data, Xinglong 2.16 m telescope spectra, and Lick 3 m Shane telescope spectra can be obtained by contacting the corresponding authors.



**Acknowledgments:** This work includes the data from LAMOST (the Large Sky Area Multi-Object Fiber Spectroscopic Telescope), which is a National Major Scientific Project built by the Chinese Academy of Sciences. Funding for the project was provided by the National Development and Reform Commission. This work made use of data from the publicly available SDSS 12 data release. Funding for the Sloan Digital Sky Survey IV was provided by the Alfred P. Sloan Foundation, the U.S. Department of Energy Office of Science, and participating institutions. SDSS IV acknowledges support and resources from the Center for High Performance Computing at the University of Utah. The SDSS website is [www.sdss4.org](http://www.sdss4.org). This paper includes data collected through the *TESS* mission, obtained from the MAST data archive at the Space Telescope Science Institute (STScI). Funding for the *TESS* mission is provided by the NASA Explorer Program. STScI is operated by the Association of Universities for Research in Astronomy, Inc., under NASA contract NAS 5–26555. We also used data from the European Space Agency (ESA) mission Gaia (<https://www.cosmos.esa.int/gaia>), processed by the Gaia Data Processing and Analysis Consortium (DPAC, <https://www.cosmos.esa.int/web/gaia/dpac/consortium>). Funding for the DPAC was provided by national institutions, in particular the institutions participating in the Gaia Multilateral Agreement. This work made use of observations obtained with the Samuel Oschin 48-inch telescope and the 60-inch telescope at Palomar Observatory as part of the Zwicky Transient Facility project. ZTF is supported by the U.S. National Science Foundation (NSF) under grants AST-1440341 and AST-2034437 and collaboration including current partners Caltech, IPAC, the Weizmann Institute for Science, the Oskar Klein Center at Stockholm University, the University of Maryland, Deutsches Elektronen-Synchrotron and Humboldt University, the TANGO Consortium of Taiwan, the University of Wisconsin at Milwaukee, Trinity College Dublin, Lawrence Livermore National Laboratories, IN2P3, University of Warwick, Ruhr University Bochum, and Northwestern University, and former partners the University of Washington, Los Alamos National Laboratories, and Lawrence Berkeley National Laboratories. Operations are conducted by COO, IPAC, and UW. This research made use of the International Variable Star Index (VSX; Watson et al. [42]) database, operated at AAVSO, Cambridge, MA, USA.

**Conflicts of Interest:** The authors declare no conflicts of interest.

Appendix A

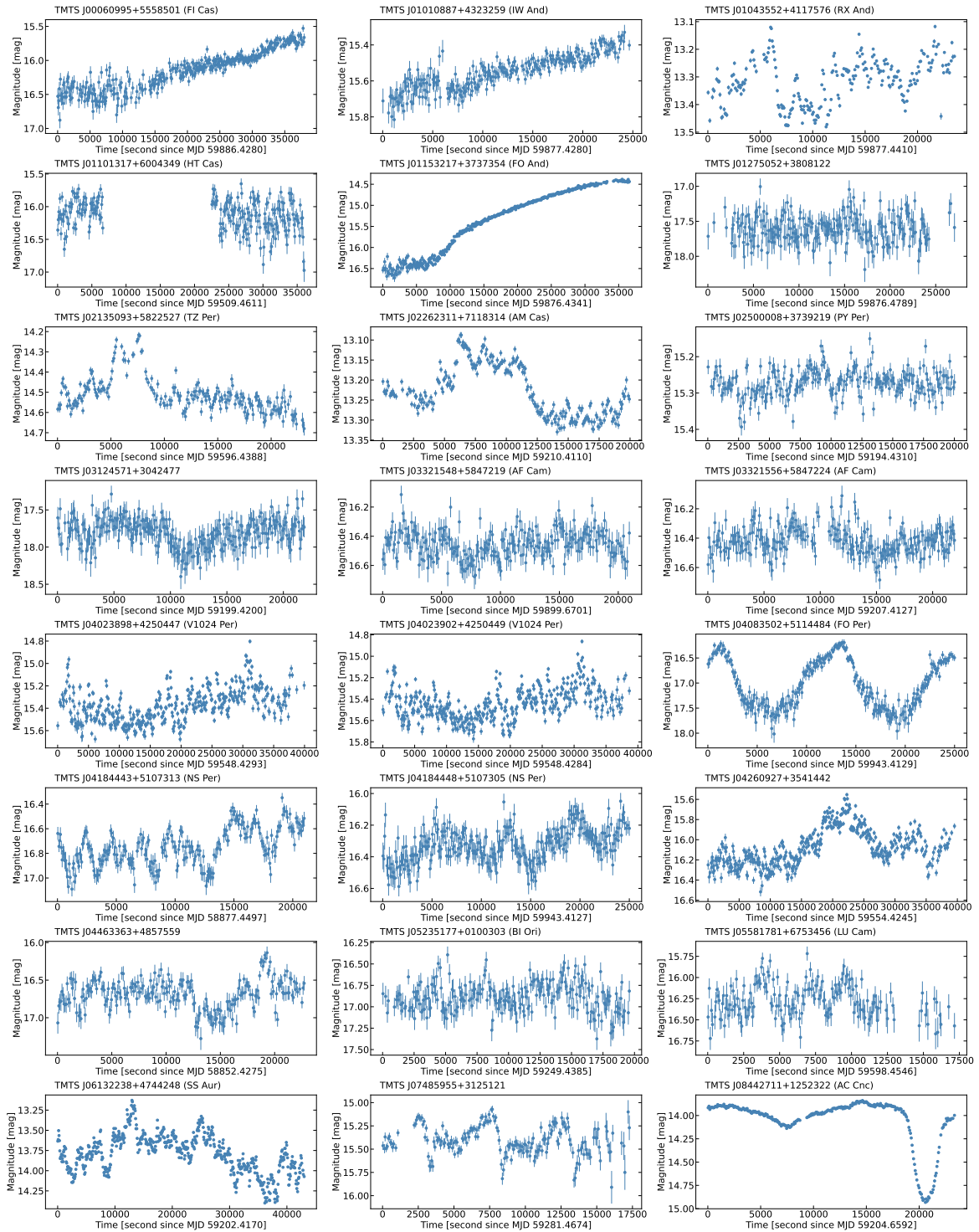
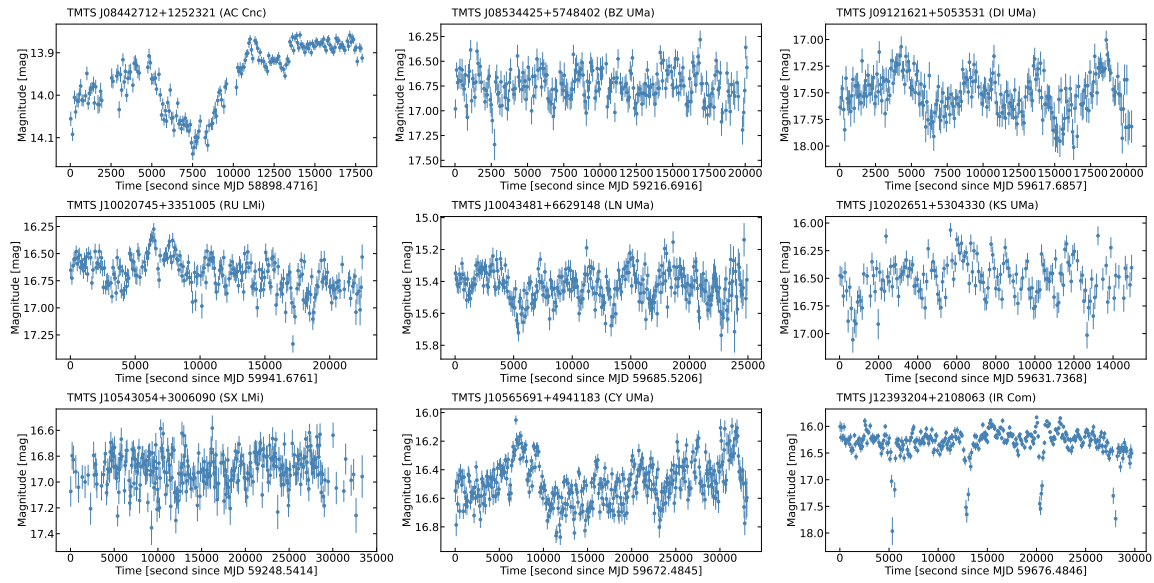
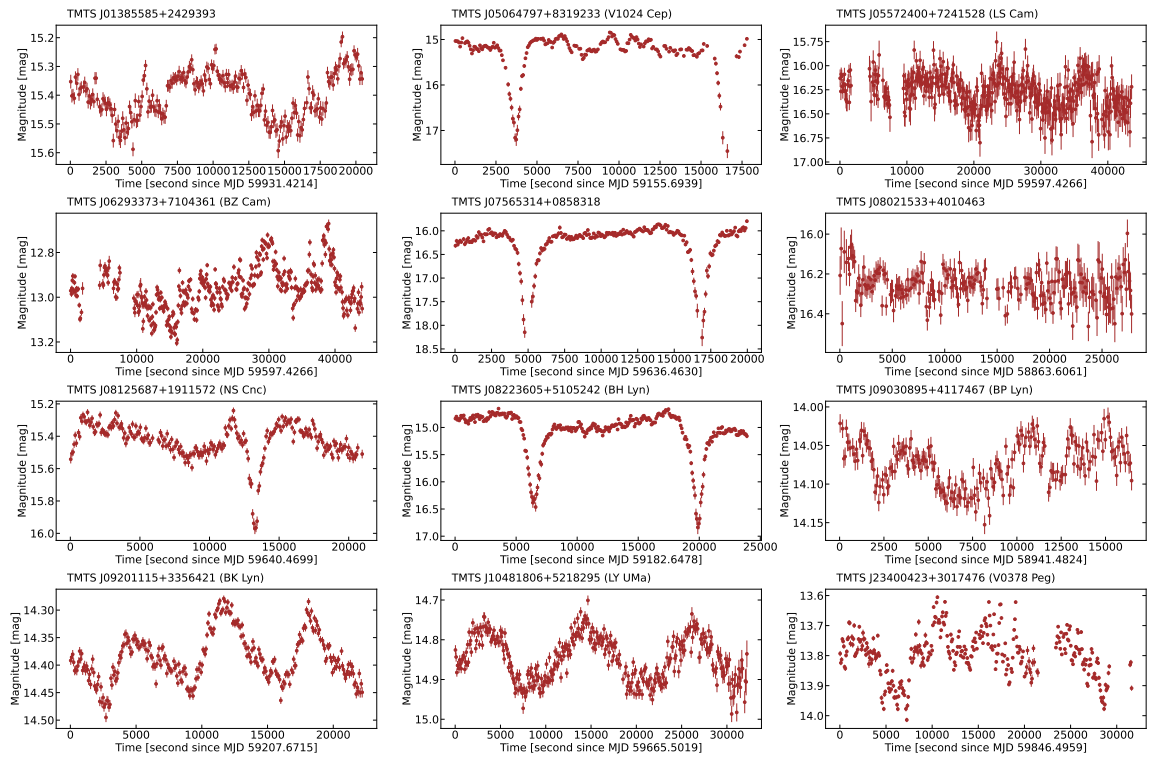


Figure A1. Cont.



**Figure A1.** Light curves of DNe presented in this work. The start time of each observation can be found in Table 1.



**Figure A2.** Light curves of NLs presented in this work. The start time of each observation can be found in Table 1.

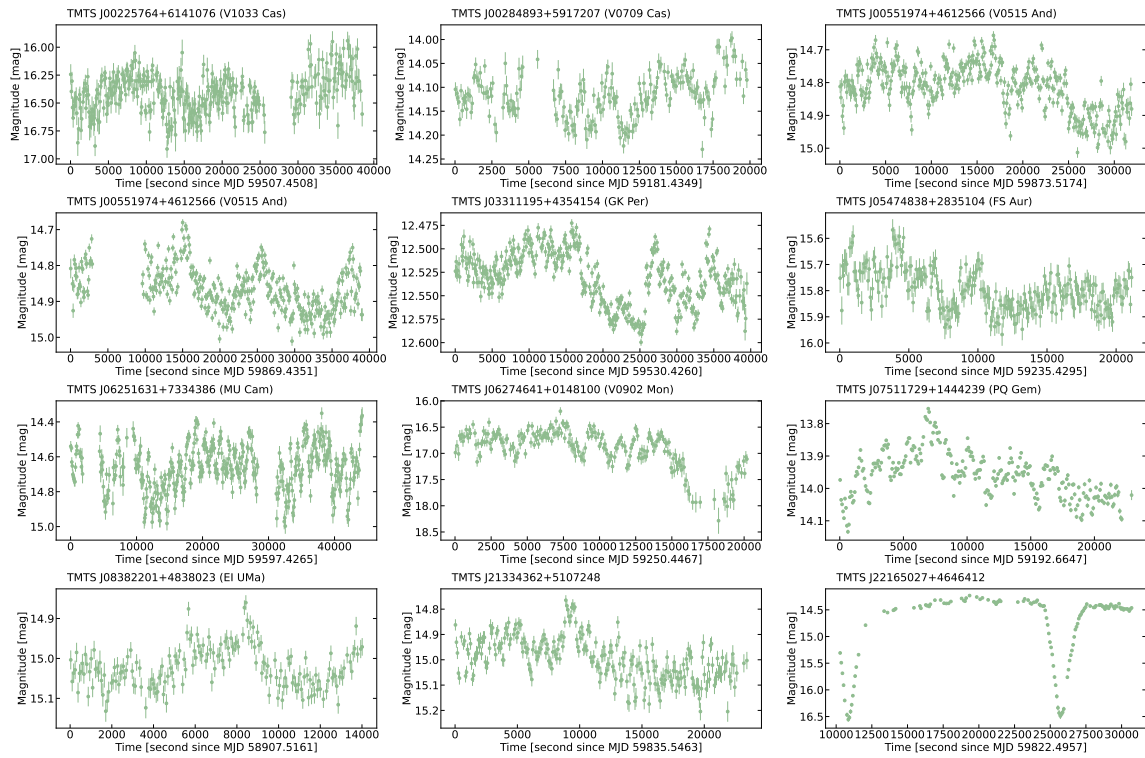


**Figure A3.** Light curves of IPs presented in this work. The start time of each observation can be found in Table 1.

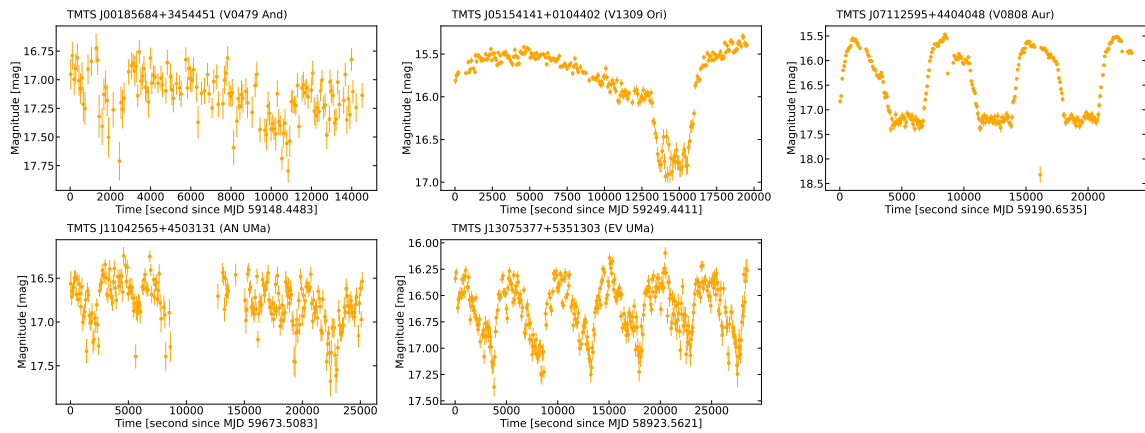


**Figure A4.** Light curves of AMs presented in this work. The start time of each observation can be found in Table 1.

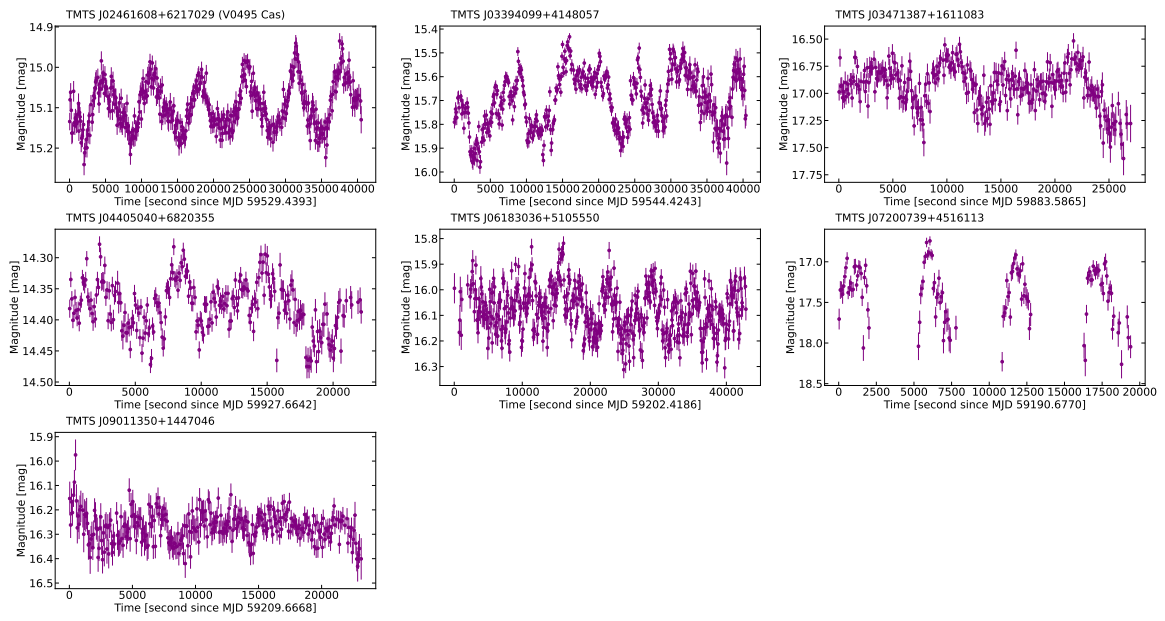


**Figure A5.** Light curves of CV candidates presented in this work. The start time of each observation can be found in Table 1.

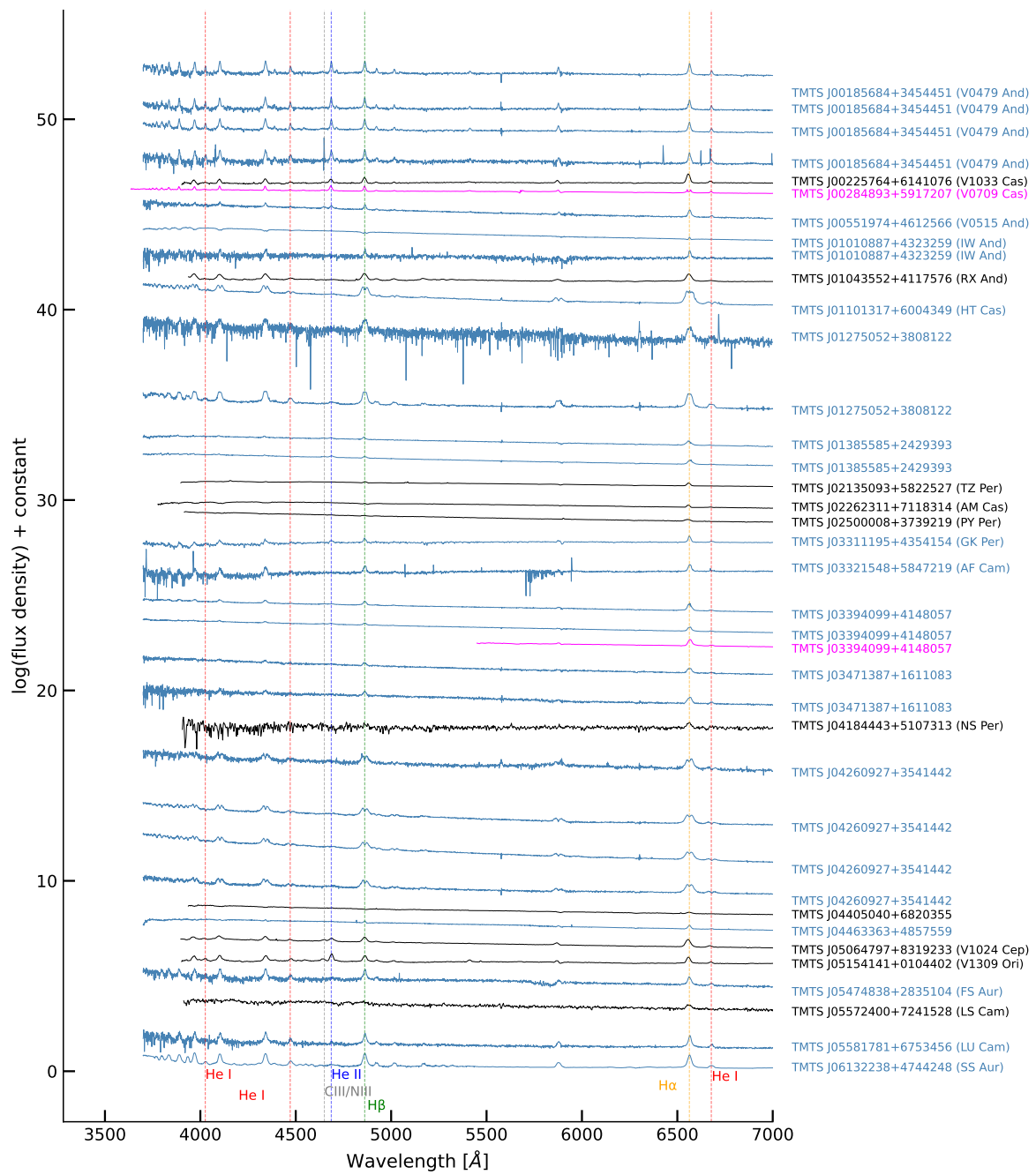
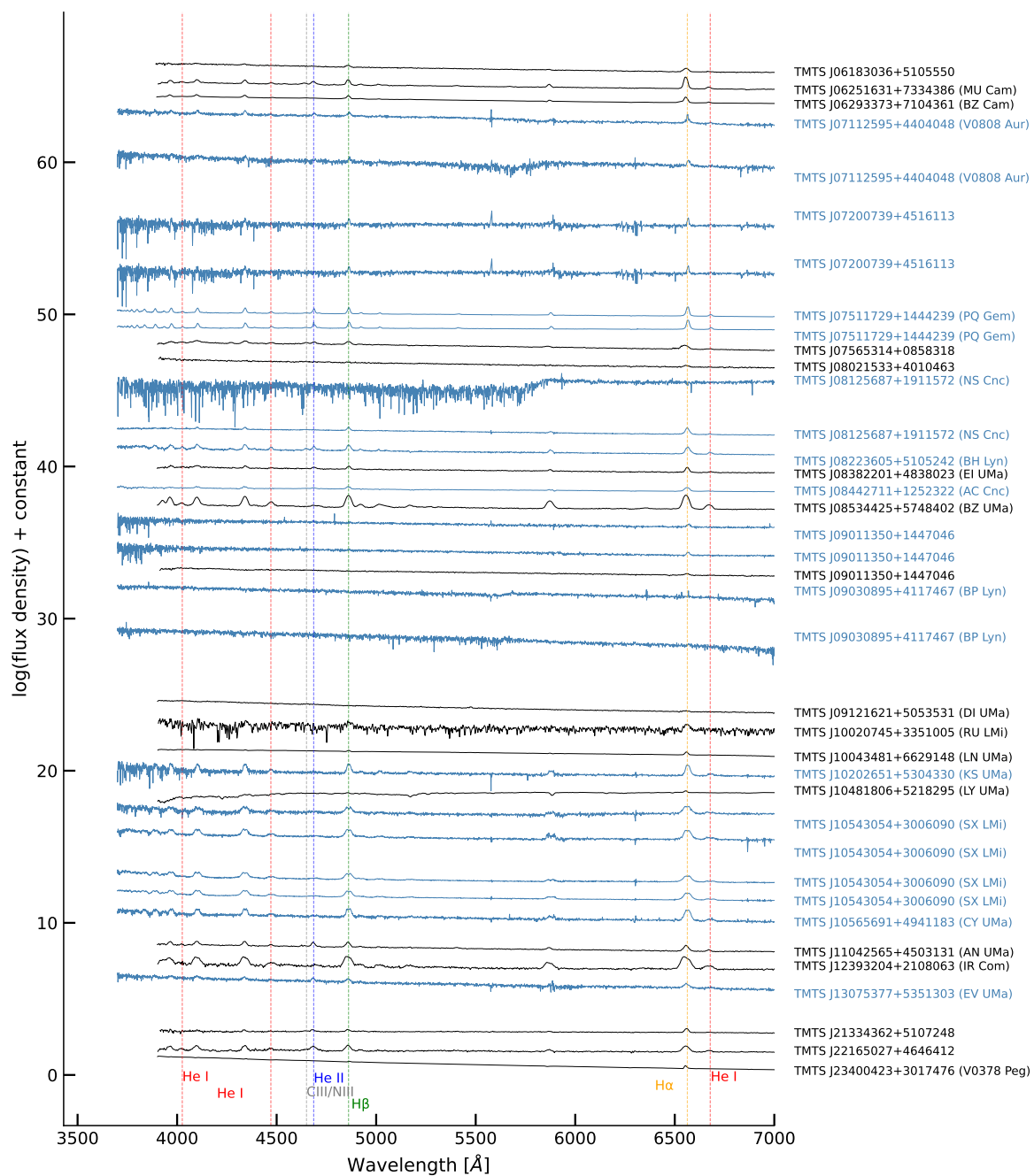


Figure A6. Cont.





**Figure A6.** Spectra of 53 cataclysmic variables mentioned in Section 2.3. The spectra taken with the Xinglong 2.16 m telescope, LAMOST, and Lick 3 m Shane telescope are shown in black, blue, and magenta colors, respectively. Some spectral characteristics are indicated with vertical dashed lines in different colors. The corresponding TMTS names are labeled on the right of each spectrum.

## References

1. Maoz, D.; Mannucci, F.; Nelemans, G. Observational Clues to the Progenitors of Type Ia Supernovae. *Annu. Rev. Astron. Astrophys.* **2014**, *52*, 107–170. <https://doi.org/10.1146/annurev-astro-082812-141031>.
2. Liu, Z.W.; Röpke, F.K.; Han, Z. Type Ia Supernova Explosions in Binary Systems: A Review. *Res. Astron. Astrophys.* **2023**, *23*, 082001. <https://doi.org/10.1088/1674-4527/acd89e>.
3. Nelemans, G.; Portegies Zwart, S.F.; Verbunt, F.; Yungelson, L.R. Population synthesis for double white dwarfs. II. Semi-detached systems: AM CVn stars. *Astron. Astrophys.* **2001**, *368*, 939–949. <https://doi.org/10.1051/0004-6361:20010049>.
4. Podsiadlowski, P.; Han, Z.; Rappaport, S. Cataclysmic variables with evolved secondaries and the progenitors of AM CVn stars. *Mon. Not. R. Astron. Soc.* **2003**, *340*, 1214–1228. <https://doi.org/10.1046/j.1365-8711.2003.06380.x>.

5. Luo, J.; Chen, L.S.; Duan, H.Z.; Gong, Y.G.; Hu, S.; Ji, J.; Liu, Q.; Mei, J.; Milyukov, V.; Sazhin, M.; et al. TianQin: A space-borne gravitational wave detector. *Class. Quantum Gravity* **2016**, *33*, 035010. <https://doi.org/10.1088/0264-9381/33/3/035010>.
6. Amaro-Seoane, P.; Audley, H.; Babak, S.; Baker, J.; Barausse, E.; Bender, P.; Berti, E.; Binetruy, P.; Born, M.; Bortoluzzi, D.; et al. Laser Interferometer Space Antenna. *arXiv* **2017**, arXiv:1702.00786. <https://doi.org/10.48550/arXiv.1702.00786>.
7. Warner, B. *Cataclysmic Variable Stars*; Cambridge Astrophysics Series; Cambridge University Press: Cambridge, UK, 1995; Volume 28.
8. Khangale, Z.N.; Woudt, P.A.; Potter, S.B.; Warner, B.; Kilkenny, D.; van der Heyden, K. A spectroscopic analysis of the eclipsing nova-like EC 21178-5417—Discovery of spiral density structures. *Mon. Not. R. Astron. Soc.* **2020**, *495*, 637–649. <https://doi.org/10.1093/mnras/staa680>.
9. Bridge, C.M.; Hakala, P.; Cropper, M.; Ramsay, G. Accretion stream mapping with ‘genetically modified fireflies’. *Mon. Not. R. Astron. Soc.* **2004**, *351*, 1423–1429. <https://doi.org/10.1111/j.1365-2966.2004.07884.x>.
10. Kennedy, M.R.; Garnavich, P.M.; Littlefield, C.; Marsh, T.R.; Callanan, P.; Breton, R.P.; Augusteijn, T.; Wagner, R.M.; Ashley, R.P.; Neric, M. Optical spectra of FO Aquarii during low and high accretion rates. *Mon. Not. R. Astron. Soc.* **2020**, *495*, 4445–4462. <https://doi.org/10.1093/mnras/staa1415>.
11. Wu, K. Accretion onto Magnetic White Dwarfs. *Space Sci. Rev.* **2000**, *93*, 611–649. <https://doi.org/10.1023/A:1026522914125>.
12. Busschaert, C.; Falize, É.; Michaut, C.; Bonnet-Bidaud, J.M.; Mouchet, M. Quasi-periodic oscillations in accreting magnetic white dwarfs. II. The asset of numerical modelling for interpreting observations. *Astron. Astrophys.* **2015**, *579*, A25. <https://doi.org/10.1051/0004-6361/201425483>.
13. Bruch, A. TESS light curves of cataclysmic variables—II—Superhumps in old novae and novalike variables. *Mon. Not. R. Astron. Soc.* **2023**, *519*, 352–376. <https://doi.org/10.1093/mnras/stac3493>.
14. Osaki, Y. Dwarf-Nova Outbursts. *Publ. Astron. Soc. Pac.* **1996**, *108*, 39. <https://doi.org/10.1086/133689>.
15. Whitehurst, R.; King, A. Superhumps, resonances and accretion discs. *Mon. Not. R. Astron. Soc.* **1991**, *249*, 25–35. <https://doi.org/10.1093/mnras/249.1.25>.
16. Wood, M.A.; Thomas, D.M.; Simpson, J.C. SPH simulations of negative (nodal) superhumps: A parametric study. *Mon. Not. R. Astron. Soc.* **2009**, *398*, 2110–2121. <https://doi.org/10.1111/j.1365-2966.2009.15252.x>.
17. Thomas, D.M.; Wood, M.A. The Emergence of Negative Superhumps in Cataclysmic Variables: Smoothed Particle Hydrodynamics Simulations. *Astrophys. J.* **2015**, *803*, 55. <https://doi.org/10.1088/0004-637X/803/2/55>.
18. Knigge, C. The donor stars of cataclysmic variables. *Mon. Not. R. Astron. Soc.* **2006**, *373*, 484–502. <https://doi.org/10.1111/j.1365-2966.2006.11096.x>.
19. Spruit, H.C.; Ritter, H. Stellar activity and the period gap in cataclysmic variables. *Astron. Astrophys.* **1983**, *124*, 267–272.
20. Patterson, J. The evolution of cataclysmic and low-mass X-ray binaries. *Astrophys. J. Suppl. Ser.* **1984**, *54*, 443–493. <https://doi.org/10.1086/190940>.
21. Williams, R.E. Emission lines from the accretion disks of cataclysmic variables. *Astrophys. J.* **1980**, *235*, 939–944. <https://doi.org/10.1086/157698>.
22. Cheng, F.H.; Lin, D.N.C. Spectral Evolution of Accretion Disks of Dwarf Novae. II. Radiative Transfer Models. *Astrophys. J.* **1989**, *337*, 432. <https://doi.org/10.1086/167114>.
23. Sarty, G.E.; Wu, K. Multivariate Characterization of Hydrogen Balmer Emission in Cataclysmic Variables. *Publ. Astron. Soc. Aust.* **2006**, *23*, 106–118. <https://doi.org/10.1071/AS06011>.
24. Koch, D.G.; Borucki, W.J.; Basri, G.; Batalha, N.M.; Brown, T.M.; Caldwell, D.; Christensen-Dalsgaard, J.; Cochran, W.D.; DeVore, E.; Dunham, E.W.; et al. Kepler Mission Design, Realized Photometric Performance, and Early Science. *Astrophys. J. Lett.* **2010**, *713*, L79–L86. <https://doi.org/10.1088/2041-8205/713/2/L79>.
25. Ricker, G.R.; Winn, J.N.; Vanderspek, R.; Latham, D.W.; Bakos, G.Á.; Bean, J.L.; Berta-Thompson, Z.K.; Brown, T.M.; Buchhave, L.; Butler, N.R.; et al. Transiting Exoplanet Survey Satellite (TESS). *J. Astron. Telesc. Instruments Syst.* **2015**, *1*, 014003. <https://doi.org/10.1117/1.JATIS.1.1.014003>.
26. Otulakowska-Hypka, M.; Olech, A.; Patterson, J. Statistical analysis of properties of dwarf novae outbursts. *Mon. Not. R. Astron. Soc.* **2016**, *460*, 2526–2541. <https://doi.org/10.1093/mnras/stw1120>.
27. Bruch, A. Flickering around the outburst cycle in Kepler dwarf novae. *Mon. Not. R. Astron. Soc.* **2022**, *509*, 4669–4678. <https://doi.org/10.1093/mnras/stab2675>.
28. Zhang, J.C.; Wang, X.F.; Mo, J.; Xi, G.B.; Lin, J.; Jiang, X.J.; Zhang, X.M.; Li, W.X.; Yan, S.Y.; Chen, Z.H.; et al. The Tsinghua University-Ma Huateng Telescopes for Survey: Overview and Performance of the System. *Publ. Astron. Soc. Pac.* **2020**, *132*, 125001. <https://doi.org/10.1088/1538-3873/abbea2>.
29. Cui, X.Q.; Zhao, Y.H.; Chu, Y.Q.; Li, G.P.; Li, Q.; Zhang, L.P.; Su, H.J.; Yao, Z.Q.; Wang, Y.N.; Xing, X.Z.; et al. The Large Sky Area Multi-Object Fiber Spectroscopic Telescope (LAMOST). *Res. Astron. Astrophys.* **2012**, *12*, 1197–1242. <https://doi.org/10.1088/1674-4527/12/9/003>.
30. Zhao, G.; Zhao, Y.H.; Chu, Y.Q.; Jing, Y.P.; Deng, L.C. LAMOST spectral survey—An overview. *Res. Astron. Astrophys.* **2012**, *12*, 723–734. <https://doi.org/10.1088/1674-4527/12/7/002>.
31. Lin, J.; Wang, X.; Mo, J.; Xi, G.; Zhang, J.; Jiang, X.; Shi, J.; Zhang, X.; Zhang, X.; Wei, Z.; et al. Minute-cadence observations of the LAMOST fields with the TMST: I. Methodology of detecting short-period variables and results from the first-year survey. *Mon. Not. R. Astron. Soc.* **2022**, *509*, 2362–2376. <https://doi.org/10.1093/mnras/stab2812>.

32. Liu, Q.; Lin, J.; Wang, X.; Gu, S.; Shi, J.; Zhang, L.; Xi, G.; Mo, J.; Cai, Y.; Chen, L.; et al. Minute-cadence observations of the LAMOST fields with the TMTS—III. Statistical study of the flare stars from the first two years. *Mon. Not. R. Astron. Soc.* **2023**, *523*, 2193–2208. <https://doi.org/10.1093/mnras/stad365>.
33. Lin, J.; Wu, C.; Xiong, H.; Wang, X.; Németh, P.; Han, Z.; Li, J.; Elias-Rosa, N.; Salmaso, I.; Filippenko, A.V.; et al. A seven-Earth-radius helium-burning star inside a 20.5-min detached binary. *Nat. Astron.* **2024**, *8*, 491–503. <https://doi.org/10.1038/s41550-023-02188-2>.
34. Lin, J.; Wu, C.; Wang, X.; Németh, P.; Xiong, H.; Wu, T.; Filippenko, A.V.; Cai, Y.; Brink, T.G.; Yan, S.; et al. An 18.9 min blue large-amplitude pulsator crossing the ‘Hertzprung gap’ of hot subdwarfs. *Nat. Astron.* **2023**, *7*, 223–233. <https://doi.org/10.1038/s41550-022-01783-z>.
35. Lin, J.; Wang, X.; Mo, J.; Xi, G.; Filippenko, A.V.; Yan, S.; Brink, T.G.; Yang, Y.; Wu, C.; Németh, P.; et al. Minute-cadence observations of the LAMOST fields with the TMTS: II. Catalogues of short-period variable stars from the first 2-yr surveys. *Mon. Not. R. Astron. Soc.* **2023**, *523*, 2172–2192. <https://doi.org/10.1093/mnras/stad994>.
36. Guo, F.; Lin, J.; Wang, X.; Chen, X.; Li, T.; Chen, L.; Xia, Q.; Mo, J.; Xi, G.; Zhang, J.; et al. Minute-cadence observations of the LAMOST Fields with the TMTS—V. Machine learning classification of TMTS catalogues of periodic variable stars. *Mon. Not. R. Astron. Soc.* **2024**, *528*, 6997–7015. <https://doi.org/10.1093/mnras/stae404>.
37. Wenger, M.; Ochsenbein, F.; Egret, D.; Dubois, P.; Bonnarel, F.; Borde, S.; Genova, F.; Jasniewicz, G.; Laloë, S.; Lesteven, S.; et al. The SIMBAD astronomical database. The CDS reference database for astronomical objects. *Astron. Astrophys. Suppl.* **2000**, *143*, 9–22. <https://doi.org/10.1051/aas:2000332>.
38. Downes, R.A.; Webbink, R.F.; Shara, M.M.; Ritter, H.; Kolb, U.; Duerbeck, H.W. A Catalog and Atlas of Cataclysmic Variables: The Living Edition. *Publ. Astron. Soc. Pac.* **2001**, *113*, 764–768. <https://doi.org/10.1086/320802>.
39. Ritter, H.; Kolb, U. Catalogue of cataclysmic binaries, low-mass X-ray binaries and related objects (Seventh edition). *Astron. Astrophys.* **2003**, *404*, 301–303. <https://doi.org/10.1051/0004-6361:20030330>.
40. Szkody, P.; Anderson, S.F.; Brooks, K.; Gänsicke, B.T.; Kronberg, M.; Riecken, T.; Ross, N.P.; Schmidt, G.D.; Schneider, D.P.; Agüeros, M.A.; et al. Cataclysmic Variables from the Sloan Digital Sky Survey. VIII. The Final Year (2007–2008). *Astron. J.* **2011**, *142*, 181. <https://doi.org/10.1088/0004-6256/142/6/181>.
41. Sun, Y.; Cheng, Z.; Ye, S.; Ding, R.; Peng, Y.; Zhang, J.; Huo, Z.; Cui, W.; Wang, X.; Shi, J.; et al. A Catalog of 323 Cataclysmic Variables from LAMOST DR6. *Astrophys. J. Suppl. Ser.* **2021**, *257*, 65. <https://doi.org/10.3847/1538-4365/ac283a>.
42. Watson, C.L.; Henden, A.A.; Price, A. The International Variable Star Index (VSX). *Soc. Astron. Sci. Annu. Symp.* **2006**, *25*, 47.
43. Hou, W.; Luo, A.I.; Li, Y.B.; Qin, L. Spectroscopically Identified Cataclysmic Variables from the LAMOST Survey. I. The Sample. *Astron. J.* **2020**, *159*, 43. <https://doi.org/10.3847/1538-3881/ab5962>.
44. Thorstensen, J.R. Follow-up Studies of Five Cataclysmic Variable Candidates Discovered by LAMOST. *Astron. J.* **2020**, *160*, 151. <https://doi.org/10.3847/1538-3881/aba7c7>.
45. Szkody, P.; Anderson, S.F.; Hayden, M.; Kronberg, M.; McGurk, R.; Riecken, T.; Schmidt, G.D.; West, A.A.; Gänsicke, B.T.; Nebot Gomez-Moran, A.; et al. Cataclysmic Variables from SDSS. VII. The Seventh Year (2006). *Astron. J.* **2009**, *137*, 4011–4019. <https://doi.org/10.1088/0004-6256/137/4/4011>.
46. Denisenko, D. MASTER OT J072007.30+451611.6: Cataclysmic Variable with an Extreme Hot Spot. *Astron. Telegr.* **2018**, *11626*, 1.
47. Drake, A.J.; Graham, M.J.; Djorgovski, S.G.; Catelan, M.; Mahabal, A.A.; Torrealba, G.; García-Álvarez, D.; Donalek, C.; Prieto, J.L.; Williams, R.; et al. The Catalina Surveys Periodic Variable Star Catalog. *Astrophys. J. Suppl. Ser.* **2014**, *213*, 9. <https://doi.org/10.1088/0067-0049/213/1/9>.
48. Osborne, J.P.; Page, K.L.; Henden, A.A.; Ness, J.-U.; Bode, M.F.; Schwarz, G.J.; Starrfield, S.; Drake, J.J.; Kuulkers, E.; Beardmore, A.P. Swift observations of the March 2011 outburst of the cataclysmic variable NSV 1436: A probable dwarf nova. *Astron. Astrophys.* **2011**, *533*, A41. <https://doi.org/10.1051/0004-6361/201117088>.
49. Denisenko, D.; Podvorotny, P.; Balanutsa, P.; Shurpakov, S.; Tiurina, N.; Gorbovskey, E.; Lipunov, V.; Kornilov, V.; Belinski, A.; Shatskiy, N.; et al. One very bright and one bright OT detected by MASTER. *Astron. Telegr.* **2012**, *4441*, 1.
50. Kato, T.; Hamsch, F.J.; Monard, B.; Vanmunster, T.; Maeda, Y.; Miller, I.; Itoh, H.; Kiyota, S.; Isogai, K.; Kimura, M.; et al. Survey of period variations of superhumps in SU UMa-type dwarf novae. VIII. The eighth year (2015–2016). *Publ. Astron. Soc. Jpn.* **2016**, *68*, 65. <https://doi.org/10.1093/pasj/psw064>.
51. Kozhevnikov, V.P. An extensive photometric study of the recently discovered intermediate polar V515 And (XSS J00564+4548). *Mon. Not. R. Astron. Soc.* **2012**, *422*, 1518–1526. <https://doi.org/10.1111/j.1365-2966.2012.20725.x>.
52. Witham, A.R.; Knigge, C.; Aungwerojwit, A.; Drew, J.E.; Gänsicke, B.T.; Greimel, R.; Groot, P.J.; Roelofs, G.H.A.; Steeghs, D.; Woudt, P.A. Newly discovered cataclysmic variables from the INT/WFC photometric H $\alpha$  survey of the northern Galactic plane. *Mon. Not. R. Astron. Soc.* **2007**, *382*, 1158–1168. <https://doi.org/10.1111/j.1365-2966.2007.12426.x>.
53. Yakin, D.G.; Suleimanov, V.F.; Vlasyuk, V.V.; Spiridonova, O.I. HBHA 4705-03: A new cataclysmic variable. *Astron. Lett.* **2013**, *39*, 38–53. <https://doi.org/10.1134/S1063773713010039>.
54. Thorne, K.; Garnavich, P.; Mohrig, K. The Polar CSS 081231:071126+440405 at a Low Accretion Rate. *Inf. Bull. Var. Stars* **2010**, *5923*, 1. <https://doi.org/10.48550/arXiv.1002.0339>.
55. Lomb, N.R. Least-Squares Frequency Analysis of Unequally Spaced Data. *Astrophys. Space Sci.* **1976**, *39*, 447–462. <https://doi.org/10.1007/BF00648343>.

56. Scargle, J.D. Studies in astronomical time series analysis. II. Statistical aspects of spectral analysis of unevenly spaced data. *Astrophys. J.* **1982**, *263*, 835–853. <https://doi.org/10.1086/160554>.
57. VanderPlas, J.T. Understanding the Lomb-Scargle Periodogram. *Astrophys. J. Suppl. Ser.* **2018**, *236*, 16. <https://doi.org/10.3847/1538-4365/aab766>.
58. Long, L.; Zhang, L.Y.; Bi, S.L.; Shi, J.; Lu, H.P.; Han, X.L.; Wang, H.; Prabhakar, M. Chromospheric Activity of Periodic Variable Stars Based on the LAMOST Low- and Medium-resolution Spectral Survey. *Astrophys. J. Suppl. Ser.* **2021**, *253*, 51. <https://doi.org/10.3847/1538-4365/abe30b>.
59. Bellm, E.C.; Kulkarni, S.R.; Graham, M.J.; Dekany, R.; Smith, R.M.; Riddle, R.; Masci, F.J.; Helou, G.; Prince, T.A.; Adams, S.M.; et al. The Zwicky Transient Facility: System Overview, Performance, and First Results. *Publ. Astron. Soc. Pac.* **2019**, *131*, 018002. <https://doi.org/10.1088/1538-3873/aae3be>.
60. Masci, F.J.; Laher, R.R.; Rusholme, B.; Shupe, D.L.; Groom, S.; Surace, J.; Jackson, E.; Monkewitz, S.; Beck, R.; Flynn, D.; et al. The Zwicky Transient Facility: Data Processing, Products, and Archive. *Publ. Astron. Soc. Pac.* **2019**, *131*, 018003. <https://doi.org/10.1088/1538-3873/aae8ac>.
61. Patra, K.C.; Yang, Y.; Brink, T.G.; Höflich, P.; Wang, L.; Filippenko, A.V.; Kasen, D.; Baade, D.; Foley, R.J.; Maund, J.R.; et al. Spectropolarimetry of the Type Ia SN 2019ein rules out significant global asphericity of the ejecta. *Mon. Not. R. Astron. Soc.* **2022**, *509*, 4058–4070. <https://doi.org/10.1093/mnras/stab3136>.
62. Piirola, V.; Hakala, P.; Coyne, G.V. The Discovery of Variable Polarization over the 13.9 Minute Spin Period of the Intermediate Polar RE 0751+14. *Astrophys. J. Lett.* **1993**, *410*, L107. <https://doi.org/10.1086/186891>.
63. Butters, O.W.; Katajainen, S.; Norton, A.J.; Lehto, H.J.; Piirola, V. Circular polarization survey of intermediate polars I. Northern targets in the range  $17\text{ h} < \text{RA} < 23\text{ h}$ . *Astron. Astrophys.* **2009**, *496*, 891–902. <https://doi.org/10.1051/0004-6361/200811058>.
64. Potter, S.B.; Romero-Colmenero, E.; Kotze, M.; Zietsman, E.; Butters, O.W.; Pekeur, N.; Buckley, D.A.H. On the spin modulated circular polarization from the intermediate polars NY Lup and IGR J15094-6649. *Mon. Not. R. Astron. Soc.* **2012**, *420*, 2596–2602. <https://doi.org/10.1111/j.1365-2966.2011.20232.x>.
65. Gentile Fusillo, N.P.; Rebassa-Mansergas, A.; Gänsicke, B.T.; Liu, X.W.; Ren, J.J.; Koester, D.; Zhan, Y.; Hou, Y.; Wang, Y.; Yang, M. An independent test of the photometric selection of white dwarf candidates using LAMOST DR3. *Mon. Not. R. Astron. Soc.* **2015**, *452*, 765–773. <https://doi.org/10.1093/mnras/stv1338>.
66. Kafka, S.; Honeycutt, R.K.; Howell, S.B.; Harrison, T.E. A Multiwavelength Study of AM Herculis during the 2002–2004 Low States. *Astron. J.* **2005**, *130*, 2852–2865. <https://doi.org/10.1086/497893>.
67. Covington, A.E.; Shaw, A.W.; Mukai, K.; Littlefield, C.; Heinke, C.O.; Plotkin, R.M.; Barrett, D.; Boardman, J.; Boyd, D.; Brincat, S.M.; et al. Investigating the Low-flux States in Six Intermediate Polars. *Astrophys. J.* **2022**, *928*, 164. <https://doi.org/10.3847/1538-4357/ac5682>.
68. Drake, A.J.; Catelan, M.; Djorgovski, S.G.; Torrealba, G.; Graham, M.J.; Mahabal, A.; Prieto, J.L.; Donalek, C.; Williams, R.; Larson, S.; et al. Evidence for a Milky Way Tidal Stream Reaching Beyond 100 kpc. *Astrophys. J.* **2013**, *765*, 154. <https://doi.org/10.1088/0004-637X/765/2/154>.
69. Hou, W.; Luo, A.L.; Dong, Y.Q.; Chen, X.L.; Bai, Z.R. Spectroscopically Identified Cataclysmic Variables from the LAMOST Survey. II. Period Estimates. *Astron. J.* **2023**, *165*, 148. <https://doi.org/10.3847/1538-3881/aca906>.
70. Morgenroth, O. 50 neue Veränderliche. *Astron. Nachrichten* **1939**, *268*, 273–276. <https://doi.org/10.1002/asna.19392681703>.
71. Bruch, A. Spectroscopy of poorly known northern dwarf novae. Part I. *Astron. Astrophys. Suppl. Ser.* **1989**, *78*, 145–159.
72. Sheets, H.A.; Thorstensen, J.R.; Peters, C.J.; Kapusta, A.B.; Taylor, C.J. Spectroscopy of Nine Cataclysmic Variable Stars. *Publ. Astron. Soc. Pac.* **2007**, *119*, 494–507. <https://doi.org/10.1086/518698>.
73. Kraft, R.P.; Luyten, W.J. Binary Stars among Cataclysmic Variables. VI. on the Mean Absolute Magnitude of U Geminorum Variables. *Astrophys. J.* **1965**, *142*, 1041. <https://doi.org/10.1086/148374>.
74. Shafter, A.W.; Harkness, R.P. Spectroscopic orbits for the dwarf novae X Leonis and SS Aurigae. *Astron. J.* **1986**, *92*, 658–663. <https://doi.org/10.1086/114198>.
75. Godon, P.; Sion, E.M. White Dwarf Photospheric Abundances in Cataclysmic Variables. I. SS Aurigae and TU Mensae. *Astrophys. J.* **2021**, *908*, 173. <https://doi.org/10.3847/1538-4357/abda47>.
76. Green, R.F.; Schmidt, M.; Liebert, J. The Palomar-Green Catalog of Ultraviolet-Excess Stellar Objects. *Astrophys. J. Suppl. Ser.* **1986**, *61*, 305. <https://doi.org/10.1086/191115>.
77. Koen, C.; Orosz, J. *IBVS* **1997**, 4539.
78. Ringwald, F.A.; Velasco, K.; Roveto, J.J.; Meyers, M.E. The orbital period and negative superhumps of the nova-like cataclysmic variable V378 Pegasi. *New Astron.* **2012**, *17*, 433–437. <https://doi.org/10.1016/j.newast.2011.11.007>.
79. Kozhevnikov, V.P. Detection of superhumps in the cataclysmic variable V378 Peg (PG 2337+300). *New Astron.* **2012**, *17*, 38–42. <https://doi.org/10.1016/j.newast.2011.06.004>.
80. Sceph, N.; Begelman, M.C.; Dexter, J. QPOs in compact binaries from small-scale eruptions in an inner magnetized disc. *Mon. Not. R. Astron. Soc.* **2021**, *500*, 1547–1556. <https://doi.org/10.1093/mnras/staa3410>.
81. Kraft, R.P. Binary Stars among Cataclysmic Variables. I. U Geminorum Stars (dwarf Novae). *Astrophys. J.* **1962**, *135*, 408. <https://doi.org/10.1086/147280>.
82. Szkody, P. Observed pulsations in dwarf novae at maximum. *Astrophys. J.* **1976**, *207*, 190–194. <https://doi.org/10.1086/154483>.



83. Warner, B.; Woudt, P.A.; Pretorius, M.L. Dwarf nova oscillations and quasi-periodic oscillations in cataclysmic variables—III. A new kind of dwarf nova oscillation, and further examples of the similarities to X-ray binaries. *Mon. Not. R. Astron. Soc.* **2003**, *344*, 1193–1209. <https://doi.org/10.1046/j.1365-8711.2003.06905.x>.
84. Wagner, R.M.; Sion, E.M.; Liebert, J.; Starrfield, S.G. Hot Subluminous Stars and Blue Objects in the Case Low-Dispersion Northern Sky Survey. I. *Astrophys. J.* **1988**, *328*, 213. <https://doi.org/10.1086/166283>.
85. Howell, S.B.; Szkody, P.; Kreidl, T.J.; Mason, K.O.; Puchnarewicz, E.M. CCD Time-Resolved Photometry of Faint Cataclysmic Variables. III. *Publ. Astron. Soc. Pac.* **1990**, *102*, 758. <https://doi.org/10.1086/132700>.
86. Howell, S.B.; Liebert, J.; Wagner, R.M. Spectroscopy of Faint Cataclysmic Variables III. *Inf. Bull. Var. Stars* **1994**, *4074*, 1.
87. Cropper, M. The Polars. *Space Sci. Rev.* **1990**, *54*, 195–295. <https://doi.org/10.1007/BF00177799>.
88. Thorstensen, J.R.; Alper, E.H.; Weil, K.E. A Trip to the Cataclysmic Binary Zoo: Detailed Follow-up of 35 Recently Discovered Systems. *Astron. J.* **2016**, *152*, 226. <https://doi.org/10.3847/1538-3881/152/6/226>.
89. Knigge, C.; Baraffe, I.; Patterson, J. The Evolution of Cataclysmic Variables as Revealed by Their Donor Stars. *Astrophys. J. Suppl. Ser.* **2011**, *194*, 28. <https://doi.org/10.1088/0067-0049/194/2/28>.
90. Pala, A.F.; Gänsicke, B.T.; Townsley, D.; Boyd, D.; Cook, M.J.; De Martino, D.; Godon, P.; Haislip, J.B.; Henden, A.A.; Hubeny, I.; et al. Effective temperatures of cataclysmic-variable white dwarfs as a probe of their evolution. *Mon. Not. R. Astron. Soc.* **2017**, *466*, 2855–2878. <https://doi.org/10.1093/mnras/stw3293>.
91. Pala, A.F.; Gänsicke, B.T.; Belloni, D.; Parsons, S.G.; Marsh, T.R.; Schreiber, M.R.; Breedt, E.; Knigge, C.; Sion, E.M.; Szkody, P.; et al. Constraining the evolution of cataclysmic variables via the masses and accretion rates of their underlying white dwarfs. *Mon. Not. R. Astron. Soc.* **2022**, *510*, 6110–6132. <https://doi.org/10.1093/mnras/stab3449>.
92. Gänsicke, B.T.; Dillon, M.; Southworth, J.; Thorstensen, J.R.; Rodríguez-Gil, P.; Aungwerojwit, A.; Marsh, T.R.; Szkody, P.; Barros, S.C.C.; Casares, J.; et al. SDSS unveils a population of intrinsically faint cataclysmic variables at the minimum orbital period. *Mon. Not. R. Astron. Soc.* **2009**, *397*, 2170–2188. <https://doi.org/10.1111/j.1365-2966.2009.15126.x>.
93. Zorotovic, M.; Schreiber, M.R.; Gänsicke, B.T. Post common envelope binaries from SDSS. XI. The white dwarf mass distributions of CVs and pre-CVs. *Astron. Astrophys.* **2011**, *536*, A42. <https://doi.org/10.1051/0004-6361/201116626>.
94. Gänsicke, B.T.; Fischer, A.; Silvotti, R.; de Martino, D. A model for the optical high state light curve of AM Herculis. *Astron. Astrophys.* **2001**, *372*, 557–562. <https://doi.org/10.1051/0004-6361:20010522>.
95. Littlefield, C.; Garnavich, P.; Magno, K.; Murison, M.; Deal, S.; McClelland, C.; Rose, B. High-Amplitude, Rapid Photometric Variation of the New Polar MASTER OT J132104.04+560957.8. *Inf. Bull. Var. Stars* **2015**, *6129*, 1. <https://doi.org/10.48550/arXiv.1412.8328>.

**Disclaimer/Publisher’s Note:** The statements, opinions and data contained in all publications are solely those of the individual author(s) and contributor(s) and not of MDPI and/or the editor(s). MDPI and/or the editor(s) disclaim responsibility for any injury to people or property resulting from any ideas, methods, instructions or products referred to in the content.